

Supplementary Information (SI) Appendix for

Joint Control of Terrestrial Gross Primary Productivity by Plant Phenology and Physiology

Jianyang Xia^{1†*}, Shuli Niu^{2†*}, Philippe Ciais³, Ivan Janssens⁴, Jiquan Chen⁵, Christof Ammann⁶, Altaf Arain⁷, Peter D. Blanken⁸, Alessandro Cescatti⁹, Damien Bonal¹⁰, Nina Buchmann¹¹, Peter S. Curtis¹², Shiping Chen¹³, Jinwei Dong¹, Lawrence B. Flanagan¹⁴, Christian Frankenberg¹⁵, Teodoro Georgiadis¹⁶, Christopher M. Gough¹⁷, Dafeng Hui¹⁸, Gerard Kiely²⁰, Jianwei Li^{1,18}, Magnus Lund²⁰, Vincenzo Magliulo²¹, Barbara Marcolla²², Lutz Merbold¹¹, Leonardo Montagnani^{23,24}, Eddy Moors²⁵, Jørgen E. Olesen²⁶, Shilong Piao²⁷, Antonio Raschi²⁸, Olivier Roupsard^{29,30}, Andrew E. Suyker³¹, Marek Urbaniak³², Francesco P. Vaccari²⁸, Andrej Varlagin³³, Timo Vesala^{34,35}, Matthew Wilkinson³⁶, Ensheng Weng³⁷, Georg Wohlfahrt^{38,39}, Liming Yan⁴⁰, Yiqi Luo^{1†*},

¹Department of Microbiology and Plant Biology, University of Oklahoma, OK, USA;

²Synthesis Research Center of Chinese Ecosystem Research Network, Key Laboratory of Ecosystem Network Observation and Modeling, Institute of Geographic Sciences and Natural Resources Research, Chinese Academy of Sciences, Beijing, China;

³Laboratoire des Sciences du Climat et de l'Environnement, CEA CNRS UVSQ, 91191 Gif sur Yvette, France;

⁴Department of Biology, University of Antwerpen, Universiteitsplein 1, 2610 Wilrijk, Belgium;

⁵Center for Global Change and Earth Observations (CGCEO), and Department of Geography, Michigan State University, MI, USA;

⁶Federal Research Station Agroscope, Climate and Air Pollution Group, Zuerich, Switzerland;

⁷School of Geography and Earth Sciences, McMaster University, Hamilton, ON, Canada L8S 4K1;

⁸Department of Geography, University of Colorado at Boulder, 260 UCB, Boulder, CO, USA;

⁹European Commission, Joint Research Center, Institute for Environment and Sustainability, Ispra, Italy;

¹⁰INRA, UMR 1137 INRA-Université de Lorraine, 54280 Champenoux, France;

¹¹Institute of Agricultural Sciences, ETH Zurich, 8092 Zurich, Switzerland

- 34 ¹²Department of Evolution, Ecology & Organismal Biology, The Ohio State University,
35 Columbus, OH, USA;
- 36 ¹³State Key Laboratory of Vegetation and Environmental Change, Institute of Botany,
37 Chinese Academy of Sciences, No.20 Nanxincun, Xiangshan, Beijing 100093, China;
- 38 ¹⁴Department of Biological Sciences, University of Lethbridge, Lethbridge, Alberta, T1K
39 3M4, Canada;
- 40 ¹⁵Jet Propulsion Laboratory, M/S 183-601, 4800 Oak Grove Drive, Pasadena, CA, USA;
- 41 ¹⁶IBIMET-CNR, Via P. Gobetti 101, 40129 Bologna, Italy;
- 42 ¹⁷Department of Biology, Virginia Commonwealth University, Richmond, VA, USA;
- 43 ¹⁸Department of Biological Sciences, Tennessee State University, TN, USA;
- 44 ¹⁹Civil and Environmental Engineering Department, and Environmental Research Institute,
45 University College Cork, Cork, Ireland;
- 46 ²⁰Department of Bioscience, Aarhus University, Frederiksborgvej 399, 4000, Roskilde,
47 Denmark;
- 48 ²¹CNR-ISAFO, Institute for Mediterranean Agricultural and Forest Systems, National
49 Research Council, via Patacca 85, 80040 Ercolano (Napoli), Italy;
- 50 ²²Sustainable Agro-ecosystems and Bioresources Department, Fondazione Edmund Mach,
51 Via E. Mach, 1 38010 S. Michele all'Adige (TN), Italy;
- 52 ²³Servizi Forestali, Provincia Autonoma di Bolzano, 39100 Bolzano, Italy;
- 53 ²⁴Faculty of Science and Technology, Free University of Bolzano, Piazza Università 5, 39100
54 Bolzano, Italy;
- 55 ²⁵ESS-CC, Alterra, Wageningen UR, PO Box 47, 6700 AA Wageningen, The Netherlands;
- 56 ²⁶Department of Agroecology, Aarhus University, Blichers Allé 20, DK-8830 Tjele,
57 Denmark;
- 58 ²⁷Department of Ecology, College of Urban and Environmental Sciences, Peking University,
59 Beijing 100871, China;
- 60 ²⁸IBIMET-CNR, Via G. Caproni 8 50145 Firenze, Italy;
- 61 ²⁹CIRAD, UMR Eco&Sols (Ecologie Fonctionnelle & Biogéochimie des Sols et des Agro-
62 écosystèmes), 34060 Montpellier, France;
- 63 ³⁰CATIE (Tropical Agricultural Centre for Research and High Education), 7170 Turrialba,
64 Costa Rica;
- 65 ³¹Hardin Hall, 3310 Holdrege Street, University of Nebraska-Lincoln, Lincoln, Nebraska,
66 USA;
- 67 ³²Department of Meteorology, Poznan University of Life Sciences, Piatkowska 94, 60649
68 Poznan, Poland;
- 69 ³³A. N. Severtsov Institute of Ecology and Evolution, Russian Academy of Sciences,
70 Leninsky pr.33, Moscow, 119071, Russia;
- 71 ³⁴Department of Physics, P.O. Box 48, FIN-00014 University of Helsinki, Finland;

³⁵Department of Forest Sciences, P.O.Box 27, FIN-00014, University of Helsinki, Finland;

³⁶Centre for Sustainable Forestry & Climate Change, Forest Research, Farnham, UK;

³⁷Department of Ecology and Evolutionary Biology, Princeton University, NJ, USA;

³⁸Institute of Ecology, University of Innsbruck, Sternwartestr. 15, 6020 Innsbruck, Austria;

³⁹European Academy of Bolzano, Drususallee 1, 39100 Bolzano, Italy;

⁴⁰School of Life Sciences, Fudan University, 220 Handan Road, Shanghai, 200433, China

[†]These authors contributed equally to this work.

*To whom correspondence should be addressed. jxia@ou.edu, sniu@igsnr.ac.cn or

yluo@ou.edu

56 pages (including cover page)

S1 Materials and Methods

S1.1 Data

S1.1.1 The FLUXNET La Thuile Database

The ecosystem-level GPP were estimated by the eddy covariance technique, a key method to measure the net ecosystem-atmosphere exchange of CO₂(1). The eddy covariance technique provides a useful tool to study the seasonal dynamics of plant-community level photosynthesis(2). We used data of gross primary productivity (GPP; positive GPP means CO₂ uptake) from 213 FLUXNET sites from the La Thuile Database (www.fluxdata.org, Table S1) in our analyses. The database was a combination of measurements from the networks Ameriflux, CarboEurope and Fluxnet-Canada, and covers the time period of 1993–2006. Data of each site-year in the database was filtered according to the methods and criteria in Reichstein *et al.*(3) and Papale *et al.*(4). Since the GPP data are not directly measured, they include some inevitable uncertainties. The sources of those uncertainties have been widely

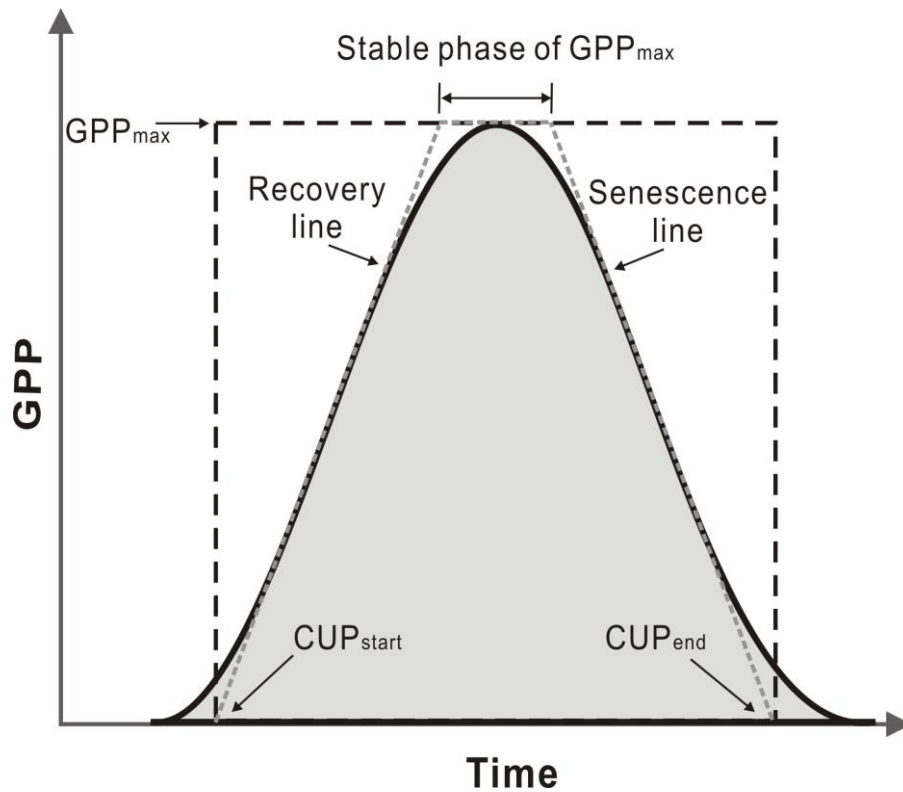
discussed by Beer *et al.*(5), Moncrieff *et al.*(6), Papale *et al.*(4), Moffat *et al.*(7) and Desai *et al.*(8). Since there is no phenological information in diurnal variations of CO₂ fixation, we used daily GPP in this study. There are some negative values for daily GPP in some site years. Only site years with more than 300 daily estimates were chosen from the database.

S1.1.2 MODIS GPP

We used the data of gross primary productivity (GPP) from the Moderate Resolution Imaging Spectroradiometer (MODIS) aboard NASA's Terra satellites (MOD17A2 GPP(9)) for North America (7.05–79.95°N, 58.55–98.85°W) during 2000-2010 in our analyses. The data set was generated by the Numerical Terradynamic Simulation Group (NTSG)/University of Montana's (UMT) as Version-55 and available from the LP DAAC(10, 11). The algorithm of MODIS GPP is described in Running *et al.*(12) and Zhao *et al.*(10). This product has considered the cloud-contamination issue while the NASA's MOD17 products (i.e., Version-5 GPP) did not. Thus, this product can avoid the underestimation in the MOD17A2-V5 products (13). The accuracy of this product has been assessed by using independent measurements made in a systematic and statistically robust way and feasible for the application of scientific community. We downloaded the data and mosaicked and re-projected the data by using the MODIS Reprojection Tool. The mosaicked images were resampled into 0.1 ° × 0.1 ° by using the nearest neighbor algorithm.

S1.2 Characteristics of annual GPP curve: definitions

In most terrestrial ecosystems, the daily GPP throughout the whole year follows a bell-shaped curve, which can be represented by the idealized solid black line in the following figure:



Supplementary Fig. S1.2.1. Ideal curve of seasonal GPP in terrestrial ecosystem.

The shape of the above unimodal curve (Fig. S1.2.1) is determined by five consecutive phases, which are described by Gu *et al.*(14):

Phase 1. Transition stage from non-growing to growing season, with a slowly increasing GPP.

Phase 2. Recover stage with rapidly increasing GPP.

Phase 3. Stable stage in the middle of the growing season, during which the plant community keeps its maximal GPP relatively stable.

Phase 4. Senescence stage with rapidly declining GPP.

Phase 5. Transition stage from growing to non-growing season, with a slowly declining GPP.

The above phases of seasonal cycle of GPP include a combination of characteristics in sequence as follows:

1. **CUP_{start}** . The start day of CO₂ uptake period during a year.
2. **Peak recovery rate of GPP**. In non-evergreen ecosystems, when plant community starts CO₂ fixation from the atmosphere in spring (or in newly started crops), the daily GPP rate recovers from 0 and gradually approaches its peak. The peak recovery rate of GPP can be obtained from the slope of the recovery line in Fig. S1.2.1.
3. **GPP_{max}** . The maximal daily GPP during the growing season.
4. **Stable phase of GPP_{max}** . The stable phase in which plant community keeps maximal GPP.
5. **Peak senescence rate of GPP**. It represents the peak rate of GPP reduction during late growing season in non-evergreen ecosystems, and can be obtained from the slope of the senescence line in Fig. S1.2.1.
6. **CUP_{end}** . The end day of CO₂ uptake period during a year.

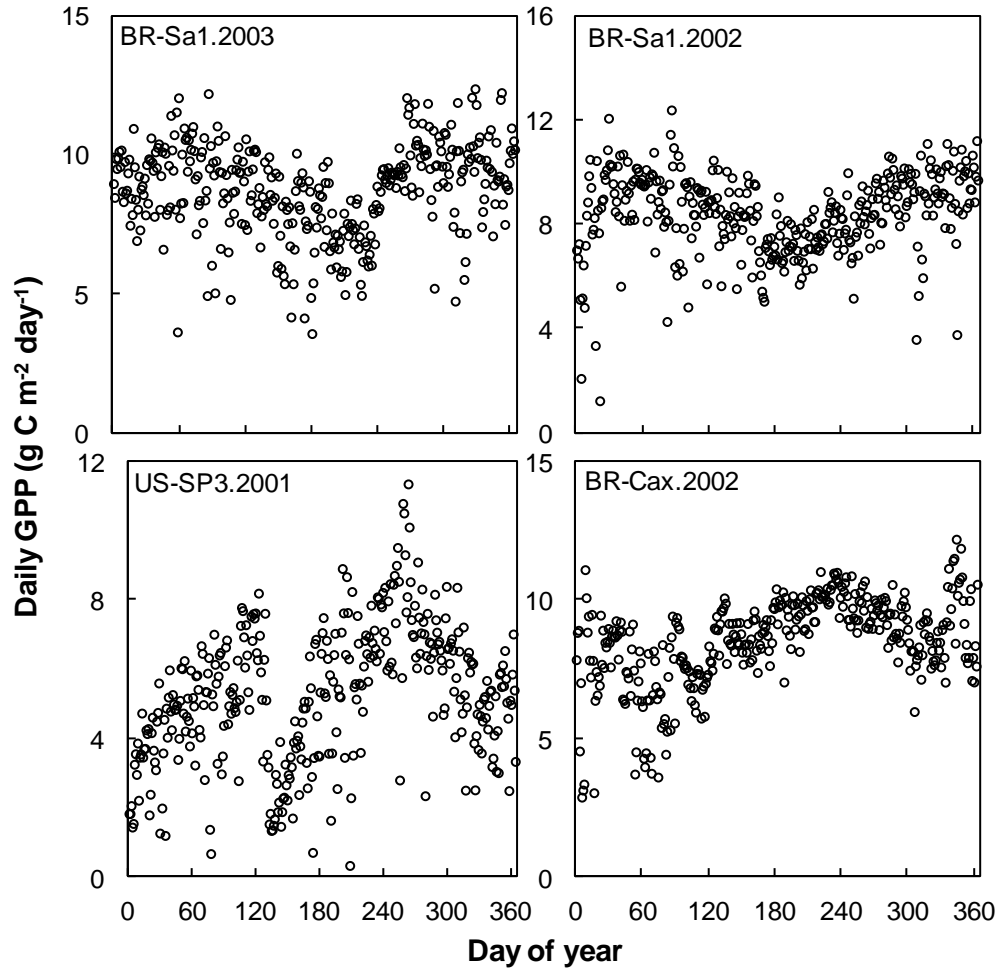
We define the CUP (carbon uptake period) as the number of days per year with $GPP > 0$. As a consequence, the CUP of an ecosystem can be calculated from CUP_{start} and CUP_{end} . CUP represents the duration of vegetation photosynthetic phenology, which is one of the functional aspects of plant phenology(14).

S1.3 Representation of the seasonal cycle of GPP

The seasonal cycle of daily GPP varies over time and across ecosystems and regions. In general, GPP seasonality in terrestrial ecosystems can be categorized into four types, including (1) one-peak during the summer-autumn growing seasons, (2) one-peak during the winter-spring seasons, (3) multiple peaks during the whole year, and (4) low seasonality such as the tropical ecosystems. Since no single function can describe the diverse GPP dynamics across the globe, we use different strategies to obtain the characteristics of annual GPP dynamics (S1.2) for each of four types of GPP seasonality above. First, we judged whether the site-year or grid cell is evergreen or not, by counting the number of days with larger daily GPP than a given value. In a second step, the number of seasons in the rest site-years or land grid cells was determined by a model function (equation 6). For those site-years and grid cells with one season, we fitted a 5-parameter Weibull function to the data from that year. For those site-years or land grid cells with more than one season, we fitted the Weibull function to each season. More details for the analyses and determinations of CUP and GPP_{max} are provided as follows:

S1.3.1. Low seasonality such as the tropical ecosystems

In some ecosystems, especially in tropical regions, the seasonality is low, and their CUP usually approaches 365 days (or 366 days in leap years). For example, as shown in Fig. S1.3.1, the dynamic of daily GPP in the sites of BR-Sa1, US-SP3 and BR-Cax does not include obvious recovery or senescence stages in a single year.



Supplementary Fig. S1.3.1. Examples of evergreen site-year with low seasonality of daily GPP . The details of the sites BR-Sa1, US-SP3 and BR-Cax can be found in Table S1.

In this study, we first judge if the site-year or grid cell is evergreen or not, by counting the number of days with larger daily GPP than a given value. Here, if there are more than 360 days with daily GPP > 1 g C m⁻² day⁻¹ in a site-year, the site-year is defined as evergreen with CUP = 365 (366 for leap years). For the MODIS GPP with the 8-day interval, we obtained daily GPP for the whole year through the linear trend between each two adjacent observations:

$$GPP(i) = GPP(i) + (i - 1) \frac{GPP(i + 1) - GPP(i)}{8} \quad (1)$$

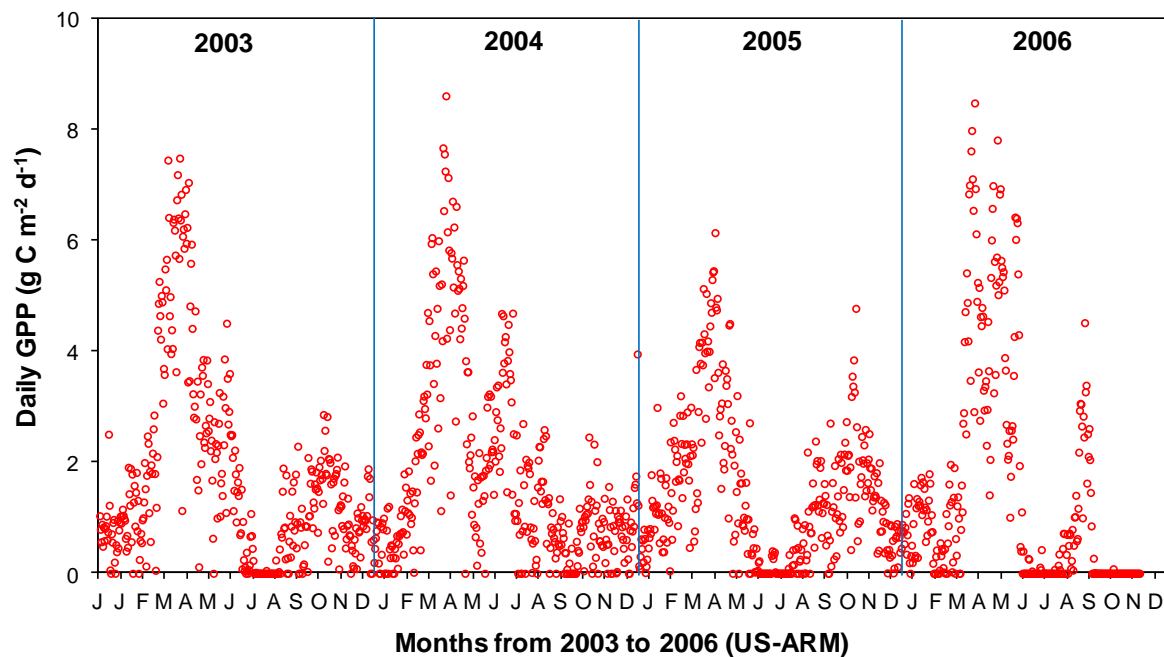
where i is the i th day of a given year.

To get the GPP_{\max} in the whole year, we first smoothed the GPP time series using a simple moving average method, which replaces the GPP in i th day of a given year (GPP_i , $i = 1, 2, \dots, N$) by a linear combination of nearby values in a window(15):

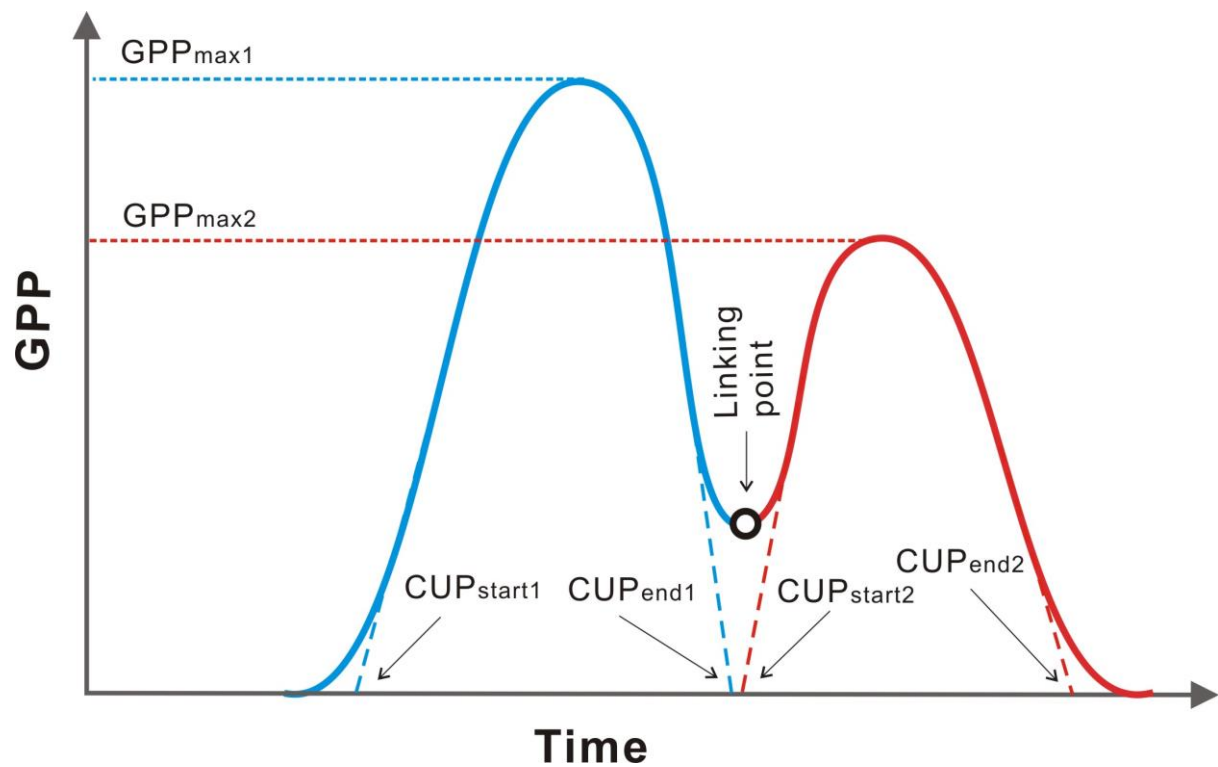
$$\sum_{j=-n}^n c_j GPP_{i+j} \quad (2)$$

where c_j represents the weighted factor and equals $1/(2n+1)$. The data of GPP_i is replaced by the values in the window calculated by the equation (2). In this study, we choose $n = 3$ to smooth the observed daily GPP. Then the maximal daily GPP was chosen as the GPP_{\max} in that year.

S1.3.2. Multiple peaks during the whole year



Supplementary Fig. S1.3.2. Observed daily GPP from 2003 to 2006 in the flux site of US-Arm (please see its details in Table S1). This figure shows there are mainly two peaks in this ecosystem, with one around April and the other in October. Note that the negative values from the database have been replaced by 0, and the observations after 324th day in 2004 were missing in the original database.



Supplementary Fig. S1.3.3. Idealized curve of GPP dynamic and its characteristics in sites with two peaks in a single year. The blue and red curve respectively represent the first and second cycle of GPP in this year.

Since sometime the two GPP cycles overlap (as shown by Fig. S1.3.3), the weighted integration of CUP from the two GPP cycles within one year was conducted as:

$$CUP = \begin{cases} CUP_1 + CUP_2 & \text{if no overlap between the two GPP cycles} \\ CUP_{end2} - CUP_{start1} & \text{if there is overlap between the two GPP cycles} \end{cases} \quad (3)$$

where CUP_1 and CUP_2 are the CO_2 uptake period in the first and second GPP cycle, respectively. CUP_{start1} is the initiation day of CUP for the first GPP cycle, and CUP_{end2} is the termination day of CUP for the second GPP cycle. The weighted integration of GPP_{max} is more complex because it depends on not only whether but also when the two GPP cycles overlap. In this study, if there is no overlap between the two GPP cycles, the yearly GPP_{max} is weighted as:

$$GPP_{max} = (GPP_{max1}CUP_1 + GPP_{max2}CUP_2)/(CUP_1 + CUP_2) \quad (4)$$

If there is overlap between the two GPP cycles, then the yearly GPP_{max} cannot be directly weighted as in equation 7. For these sites, we first find out the linking day (D_{link}) between the two GPP cycles (see the black circle in Fig. S1.3.3). Then, the weighted GPP_{max} was calculated as:

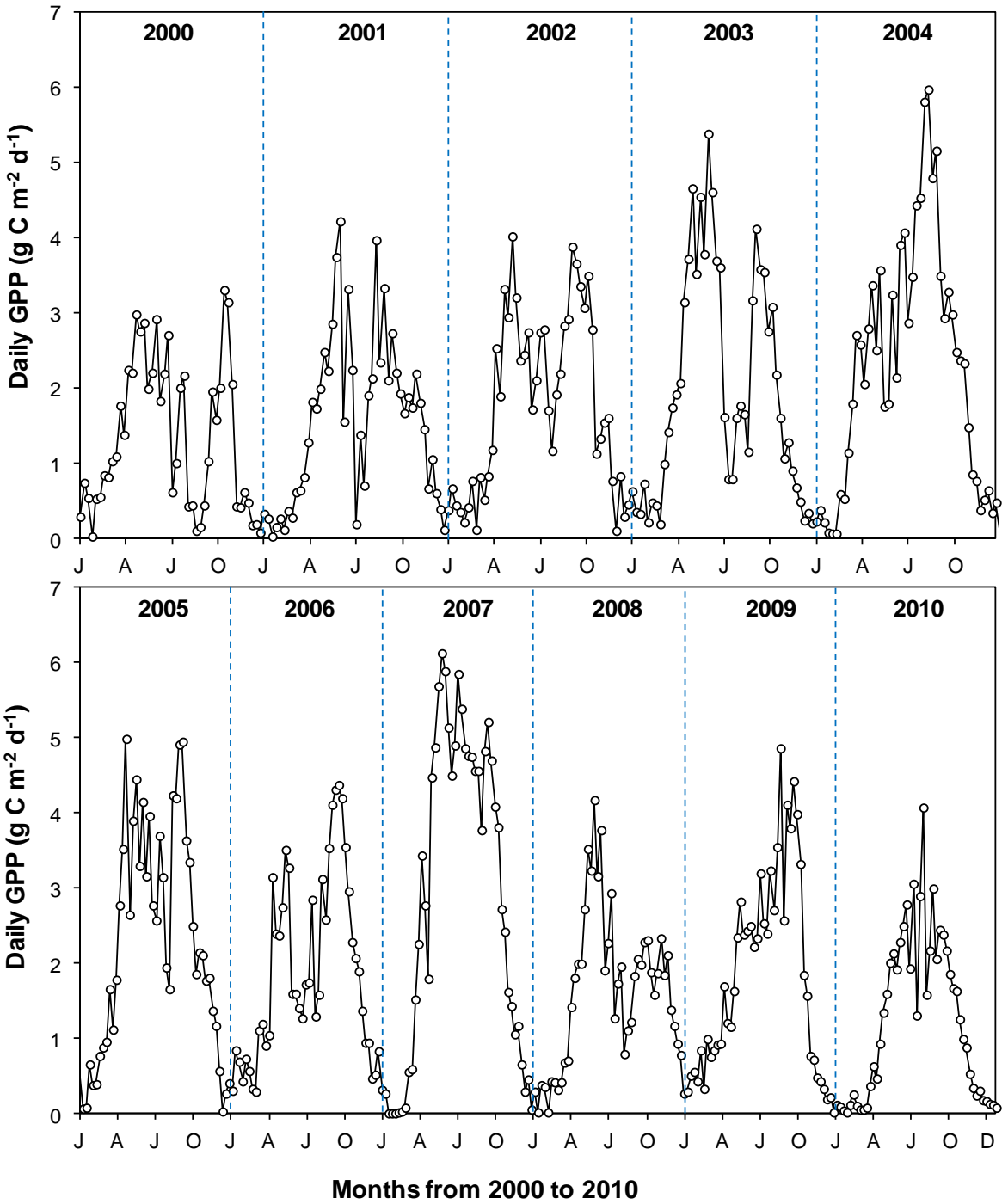
$$GPP_{max} = \frac{GPP_{max1}(D_{link} - CUP_{start1}) + GPP_{max2}(CUP_{end2} - D_{link})}{CUP_1 + CUP_2} \quad (5)$$

The same strategy as the above equations has been used if there are more than two growing seasons. Thus, one of the key steps in analyzing the GPP data in sites with multiple peaks in a single year is to determine the number of seasons. However, the GPP observations often have

high-level noise (as shown by Fig. S1.3.2, S1.3.4 and S1.3.5), making it difficult to determine the number of seasons with only one year of data(19). In this study, we reduced the risk for erroneous determination of season number by triplicating the yearly GPP dynamic (see the gray circles in Fig. S1.3.5). Then, we followed the method that is used in the TIMESAT software(19), by fitting the daily GPP data (t_i, GPP_i), $i = 1, 2, \dots, n$ for all 3 years (as shown in Fig. S1.3.5) to the following function:

$$f(t) = c_1 + c_2 \sin(\omega t) + c_3 \cos(\omega t) + c_4 \sin(2\omega t) + c_4 \cos(2\omega t) \quad (6)$$

where $\omega = 6\pi/n$. C_1 determines the base level, while $c_2 \sin(\omega t) + c_3 \cos(\omega t)$ and $c_4 \sin(2\omega t) + c_4 \cos(2\omega t)$ determine the number of seasons as one and two, respectively. During the fitting, a primary maximum is always found and a secondary maximum may be found. As suggested by TIMESAT(19), the amplitude ratio between the secondary maximum and the primary maximum can be used as an index to determine the number of vegetation seasons. That is, if the ratio is below a given threshold, the ecosystem has one season during the year. In this study, we set the ratio between the secondary maximum and the primary maximum as 0.25. For example, as shown in Fig. S1.3.5, the fitted secondary and primary maximum in 2000 in the grid of N37.75°, W101.05° are 1.69 and 2.68 g C m⁻² d⁻¹, respectively, and the ratio between them is 0.63. It means there are two vegetation seasons in this grid cell in 2000 (Fig. S1.3.5).

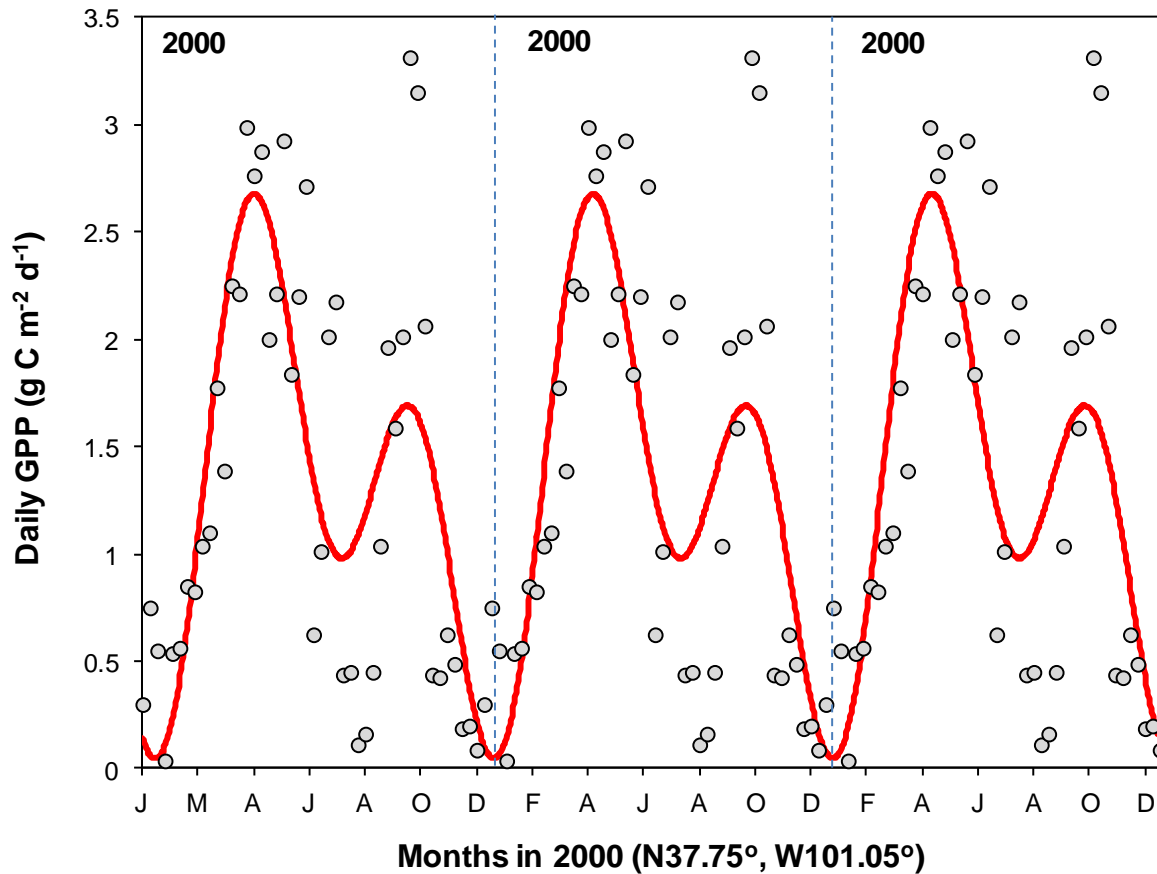


250

251

252

Supplementary Fig. S1.3.4. MODIS daily GPP from 2000 to 2010 in the grid cell of N37.75°, W101.05°. The data in the original database were in 8-day interval.



Supplementary Fig. S1.3.5. Triplicate of MODIS GPP in 2000 in the grid cell of N37.75°, W101.05° . The gray circles are the 8-day interval GPP values from the original database. The red line is the fitted GPP dynamic with the equation (6).

S1.3.3. One-peak during the summer-autumn growing seasons

In many terrestrial ecosystems, vegetation season peaks around the middle of growing season, and the seasonal cycles of daily GPP can be represented by the idealized curve in Fig. S1.2.1. In order to obtain all the characteristics (see S1.2) from both FLUXNET and MODIS-based GPP, we fitted a 5-parameter Weibull function to the data from each year. The Weibull function is given as:

$$P(t) = \begin{cases} y_0 + a \left(\frac{c-1}{c} \right)^{\frac{1-c}{c}} \left(\left| \frac{t-x_0}{b} + \left(\frac{c-1}{c} \right)^{\frac{1}{c}} \right|^{c-1} e^{\left(-\left| \frac{t-x_0}{b} + \left(\frac{c-1}{c} \right)^{\frac{1}{c}} \right|^{\frac{1}{c}} + \frac{c-1}{c} \right)} & \text{if } t \leq x_0 - b \frac{c-1}{c} \\ y_0 & \text{if } t > x_0 - b \frac{c-1}{c} \end{cases} \quad (7)$$

where t represents the number of days in each year, and $P(t)$ is the corresponding daily mean GPP ($\text{g C m}^{-2} \text{ day}^{-1}$); x_0 , y_0 , a , b , and c are empirical parameters to be estimated. As shown below, this function is flexible and fits one-peak seasonal GPP well in contrasting biomes and years. Similar Weibull functions have been successfully applied to fit seasonal dynamics of plant community photosynthesis. For example, Gu *et al.*(2) used a Weibull function to fit the seasonal cycle of plant community photosynthesis separately by dividing the growing season in its middle peak. Recently, Gu *et al.*(14) developed a new 9-parameter Weibull function capable of capturing both recovery and senescence parts of the growing season. The Weibull function used in this study captures both recovery and senescence parts of GPP dynamics, and consists of fewer empirical parameters (equation 7; 5 parameters). It has been used as a default function to fit one-peak time-series data in the Sigmaplot (Systat Software, Inc, San Jose, CA, USA).

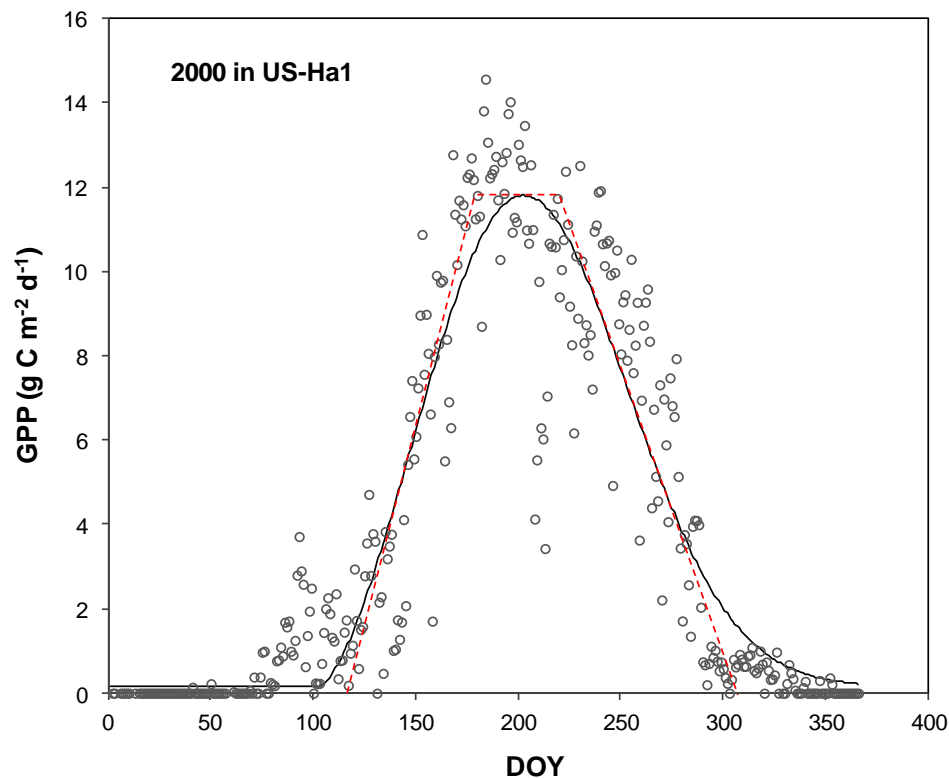
The fitting of data to the equation 7 was conducted in the R software (version 2.13.0; <http://www.R-project.org>). The details of the model fitting with nonlinear regression can be found in the section S1.4. After the curve fitting, we can obtain the fitted daily GPP in a given year. The maximal daily GPP (GPP_{\max}) is obtained as:

$$GPP_{\max} = \max \{P(t)\} \quad (8)$$

where $P(t)$ ($t = 1, 2, \dots, n$) is the daily GPP in the t th day, and n is 365 for regular years and 366 for leap years. The CO_2 uptake period (CUP) is determined by the initiation (CUP_{start}) and termination (CUP_{end}) days of CUP as:

$$CUP = CUP_{\text{end}} - CUP_{\text{start}} \quad (9)$$

Since plant community photosynthesis usually fluctuates at the start and end of CUP (as shown in the Fig. S1.3.6), it is difficult to determine the days in which the ecosystem starts or stops the CO₂ uptake. In this study, we calculated the CUP_{start} as the intersection between the recovery line (see the left red dashed line in Fig. S1.3.6) and the time (day of year) axis. Similarly, the CUP_{end} was obtained by the intersection between the senescence line (see the right red dashed line in Fig. S1.3.6) and the time axis. Previous studies (2, 14) have found this approximation can capture the initiation and termination days of plant community photosynthesis in most terrestrial ecosystems. Thus, in order to calculate the CUP_{start} and CUP_{end}, we need to first get the recovery and senescence lines.



Supplementary Fig. S1.3.6. An example of fitting the equation 7 to GPP observations from US-Ha1 in 2000. The black solid line is the fitted curve. The red dashed lines represent recovery, stable phase of GPP_{max}, and senescence line in sequence.

The recovery and senescence lines represent the maximum and minimum in the growth rate of daily GPP, respectively. Here, we use a moving linear regression approach to seek the day in which the growth rate of daily GPP reaches maximum and minimum. The linear model used in estimating the growth rate of daily GPP is:

$$P(t) = \beta t + \beta_0 \quad (10)$$

where β is the theoretical slope representing the growth rate of daily GPP, and β_0 is the theoretical y-intercept. We conducted the linear regression analysis for day t by using the data from day $t - 3$ to $t + 3$ ($3 < t < m - 3$; m is 365 in regular years and 366 in leap years). The slope β in each day can be estimated by:

$$\hat{\beta}(t) = \frac{7 \sum_{i=t-3}^{t+3} iP(i) - \sum_{i=t-3}^{t+3} i \sum_{i=t-3}^{t+3} P(i)}{7 \sum_{i=t-3}^{t+3} i^2 - (\sum_{i=t-3}^{t+3} i)^2} \quad (11)$$

The maximal (R_{\max}) and minimal (R_{\min}) change rate of daily GPP are obtained by:

$$R_{\max} = \max \{\hat{\beta}(t)\} \quad (12)$$

$$R_{\min} = \min \{\hat{\beta}(t)\} \quad (13)$$

The associated t with R_{\max} and R_{\min} are the days (t_{\max} and t_{\min}) in which maximal and minimal change rate of daily GPP occurred, respectively. Note that the value of R_{\max} is positive and R_{\min} is negative. Thus, the CUP_{start} and CUP_{end} can be calculated as:

$$CUP_{\text{start}} = t_{\max} - \frac{P(t_{\max})}{R_{\max}} \quad (14)$$

$$CUP_{\text{end}} = t_{\min} - \frac{P(t_{\min})}{R_{\min}} \quad (15)$$

Similarly, the stable phase of GPP_{\max} (SP_{gppmax}) can be calculated as:

$$SP_{\text{gppmax}} = SP_{\text{gppmax_end}} - SP_{\text{gppmax_start}} \quad (16)$$

where SP_{gppmax_start} and SP_{gppmax_end} are the start and end days of SP_{gppmax} , and can be solved by:

$$SP_{gppmax_start} = t_{max} + \frac{GPP_{max} - P(t_{max})}{R_{max}} \quad (17)$$

$$SP_{gppmax_end} = t_{min} + \frac{GPP_{max} - P(t_{min})}{R_{min}} \quad (18)$$

The main aim of this study is to examine the dependence of annual GPP on CUP and GPP_{max} . Such dependence can be represented by the ratio (α) between annual GPP and the product of CUP and GPP_{max} as:

$$\alpha = \frac{Annual\ GPP}{CUP \times GPP_{max}} \quad (19)$$

where the annual GPP is the sum of daily GPP from the original observed data.

S1.3.4. One-peak during the winter-spring seasons

In some ecosystems, the peak of daily GPP does not occur during summer-autumn seasons, but in winter or spring. For example, in some (semi-) arid regions with the Mediterranean climate, plant photosynthesis is high in mild/wet winter and spring and is low in hot/dry summer(20). As shown by Fig. S1.3.7, the daily GPP recovers in autumn, peaks in spring, and senesces in summer in the Yatir forest (IL-Yat; 31 °20'N, 35 °03'E), which is located between three distinct landscapes, including Hebron mountains, Beersheba plateau/Negev desert, and the Judean Desert and the Dead Sea Valley(21). For these sites and grids, a direct application of the equation 7 cannot capture the CUP. In the IL-Yat case, the

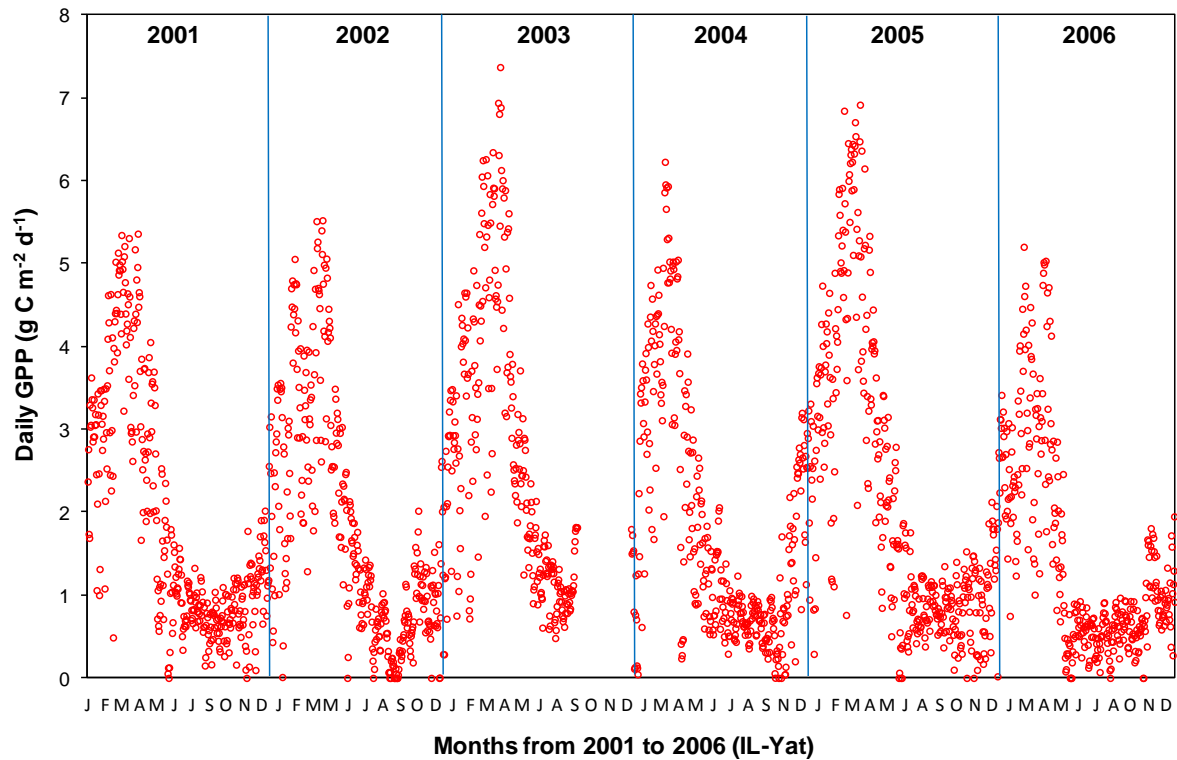
CUP will be underestimated because the CO₂ uptake period during September-December is ignored (Fig. S1.3.7).

For those sites and grids whose daily GPP peaks during spring or winter seasons, we obtained the entire growing season by duplicating the GPP dynamics (as shown by Fig. S1.3.8). As shown in Fig. S1.3.8, with the duplicate of daily GPP in 2001, an adjusted GPP dynamic can be obtained from August to July (as shown in red circles in Fig. S1.3.8). A key issue in this method is to determine the start and end day of the adjusted GPP dynamic. Since the FLUXNET GPP data are usually fluctuating with time, we determined the start and end day of the adjusted GPP dynamic by two steps:

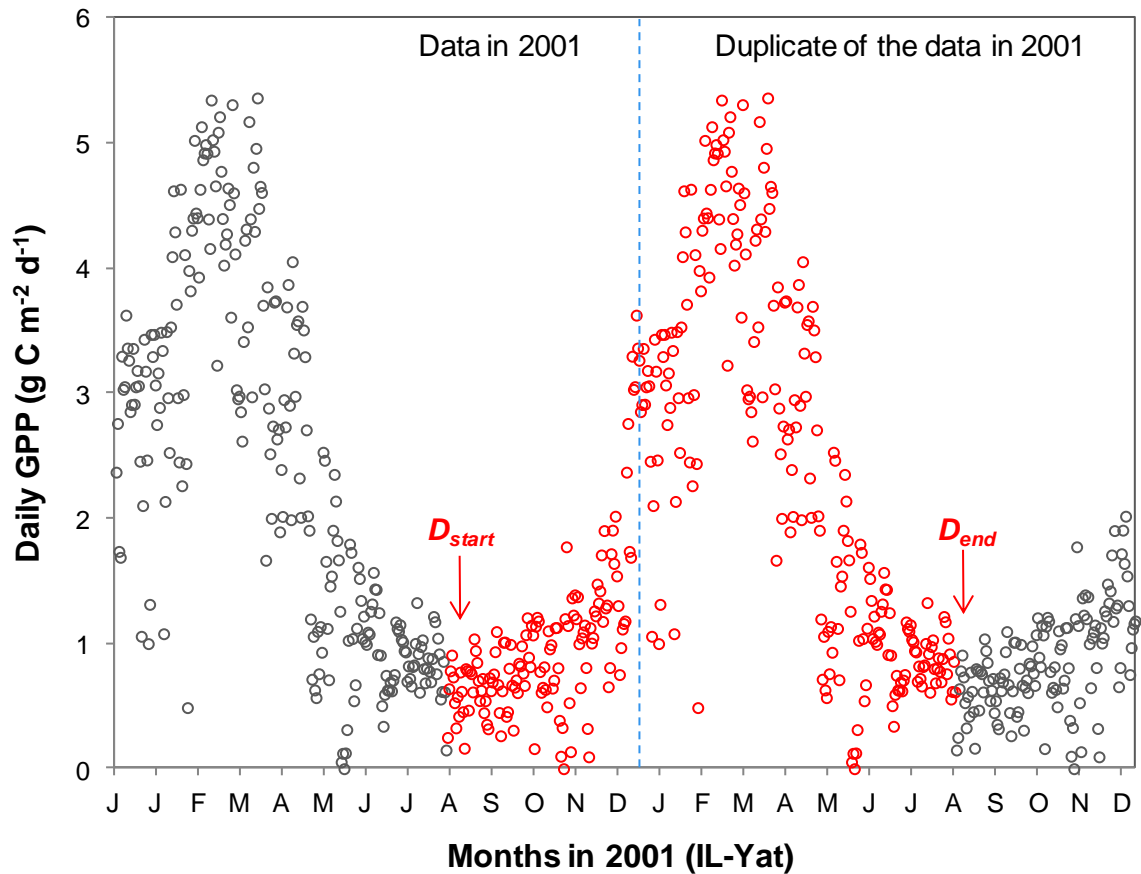
(1) We first smooth the observed data by using a moving average method as equation 2 with $n=3$.

(2) Based on the smoothed curve in the step (1), we determined the start point of the adjusted GPP dynamic as the day (D_{start}) with the minimum GPP throughout the year, and the end day (D_{end}) according to the number of days in that year.

In the MODIS GPP product, the GPP dynamic with 8-day intervals is comparably smoother, so we only applied step (2) to get the adjusted GPP dynamic. The above adjusted GPP dynamic was then used for the analysis of CUP and GPP_{max} as the regular one-peak GPP curve in the Fig. S1.3.6. Although this method with adjusted GPP dynamic may generate some errors, it can provide a good estimation of CUP and GPP_{max} for those regions in where the single peak of daily GPP occurs in winter or spring seasons.



Supplementary Fig. S1.3.7. Observed daily GPP from 2001 to 2006 at the flux site of IL-Yat (please see its details in Table S1). Note that the negative values from the database has been replaced by 0, and the observations in Oct-Dec, 2004 were missing in the original database.



Supplementary Fig. S1.3.8. The figure shows how GPP data from those sites with winter-spring peaks were adjusted and analyzed in this study. The open circles on the left side of the blue dashed line are observed daily GPP in 2001 in IL-Yat site, and those on the right side of the blue dashed line are duplicated from the observed data in 2001. Then the red open circles represent the adjusted GPP dynamic and are used in the analysis of CUP and GPP_{max} in 2001 for IL-Yat. Note that the negative values from the database have been replaced by 0.

S1.4 Non-linear regression with R

As shown in both the equations 6 and 7, there are 5 unknown parameters determining the GPP dynamic against time in a given year. In this study, we used the general normal

nonlinear regression model to fit the equations 6 and 7 to the observations. In general, the nonlinear regression model can be written as:

$$y_i = f(X_i, \beta) + \varepsilon_i \quad (21)$$

where y_i is the observed GPP in each year, f is the expectation function, and X_i is a vector of time (days in a single year). β is a vector including the 5 parameters in the equations 6 and 7, and ε_i is the error term for observation i . The error ε_i varies from year to year, and the errors are assumed to be normally distributed with mean 0 and constant variance: $\varepsilon_i \sim N(0, \sigma^2)$.

The best estimates of the parameters (β) represent the best fit of the f function to the observations y_i . They can be obtained by minimization of the sum of squared residuals (S) with respect to β :

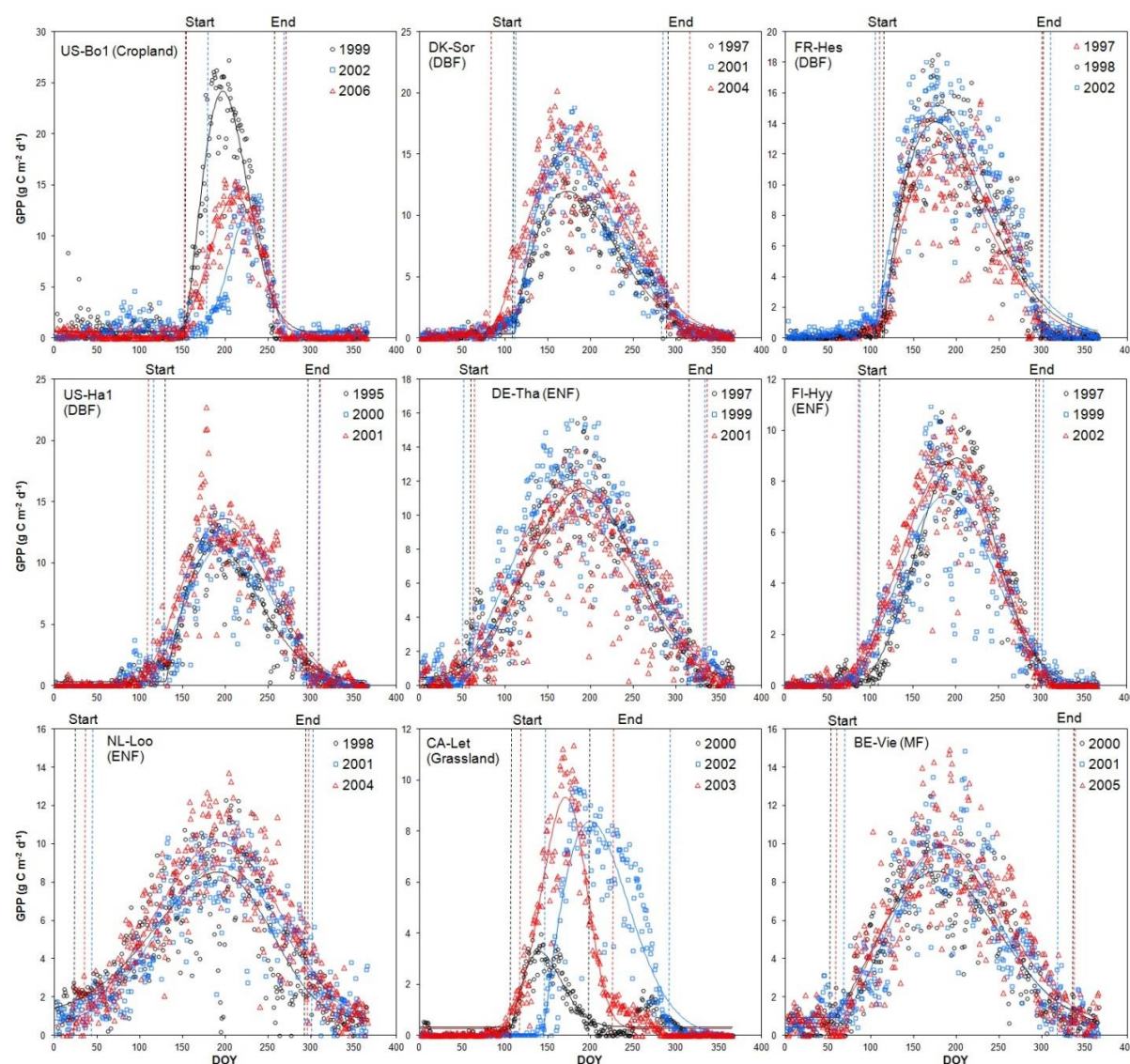
$$S(\beta) = \sum_{i=1}^n (y_i - f(X_i, \beta))^2 \quad (22)$$

In each step, the Gauss-Newton method is used to determine the new parameters values based on the data, with the purpose to make the $S(\beta)$ as small as possible. More information about the nonlinear regression can be found in Bates and Watts (22) and Fox(23).

In this study, the non-linear regressions were performed with the model fitting function *nls*, which is located in the standard *nls* library in **R**. The parameter estimates are obtained from the non-linear model fitting, and then used for the analyses of GPP properties in S1.3.

S1.5 The performance of the Weibull function in capturing GPP dynamics in terrestrial ecosystem

Since GPP dynamics in many terrestrial ecosystems follow the single-peak curve like Fig. S1.3.6, it is important to make sure that equation 7 can capture GPP properties in contrasting biomes. Before we applied the equation 7 to all flux sites and grid cells, we first examined its performance in the years with contrasting climate conditions at long-term flux sites. The results show that the equation can well capture all years of GPP dynamics from those long-term sites. As shown by Fig. S1.5.1, the simulated GPP curve fits observations from years with highest, normal, and lowest values in each site well. It indicates the Weibull function used in this study has the ability to capture GPP dynamics and the associated properties in contrasting biomes and climate conditions.



Supplementary Fig. S1.5.1. Performance of the Weibull function in fitting the GPP dynamics with lowest (black circles and lines), median (blue circles and lines) and highest (red circles and lines) annual GPP in those long-term flux sites. The dashed vertical lines represent the start and end days of CUP.

S1.6 Parameter sensitivity analysis of the Weibull function

In order to test if the convergence of α is a mathematical certainty of the Weibull function, we performed a sensitivity analysis to evaluate impact of each parameter (x_0 , y_0 , a , b , and c) on the estimates of CUP, GPP_{\max} , $CUP \times GPP_{\max}$, and α . The mathematical derivation of the sensitivity analysis can be found as follows:

We first assume $v = \left| \frac{t-x_0}{b} + \left(\frac{c-1}{c} \right)^{\frac{1}{c}} \right|$, so then the above equation can be rewritten as:

$$P(t) = \begin{cases} y_0 + a \left(\frac{c-1}{c} \right)^{\frac{1-c}{c}} v^{c-1} e^{(-v^c + \frac{c-1}{c})} & \text{if } t \leq x_0 - b \frac{c-1}{c} \\ y_0 & \text{if } t > x_0 - b \frac{c-1}{c} \end{cases} \quad (23)$$

$P(t)$ is a differentiable function whose derivative is:

$$P(t)' = \begin{cases} a \left(\frac{c-1}{c} \right)^{\frac{1-c}{c}} e^{\frac{c-1}{c}} (v^{c-1} e^{-v^c})' v' & \text{if } x \leq x_0 - b \frac{c-1}{c} \\ 0 & \text{if } x > x_0 - b \frac{c-1}{c} \end{cases}$$

$$\Rightarrow P(t)' = \begin{cases} a \left(\frac{c-1}{c} \right)^{\frac{1-c}{c}} e^{\frac{c-1}{c}} (v^{c-1} e^{-v^c})' v' & \text{if } x \leq x_0 - b \frac{c-1}{c} \\ 0 & \text{if } x > x_0 - b \frac{c-1}{c} \end{cases}$$

$$\Rightarrow P(t)' = \begin{cases} a \left(\frac{c-1}{c} \right)^{\frac{1-c}{c}} e^{\frac{c-1}{c}} [(c-1)v^{c-2} e^{-v^c} - cv^{2(c-1)} e^{-v^c}] v' & \text{if } x \leq x_0 - b \frac{c-1}{c} \\ 0 & \text{if } x > x_0 - b \frac{c-1}{c} \end{cases} \quad (24)$$

$$\text{where } v' = \begin{cases} \frac{1}{b} & \text{if } \frac{x-x_0}{b} + \left(\frac{c-1}{c} \right)^{\frac{1}{c}} \geq 0 \\ -\frac{1}{b} & \text{if } \frac{x-x_0}{b} + \left(\frac{c-1}{c} \right)^{\frac{1}{c}} < 0 \end{cases} \quad (25)$$

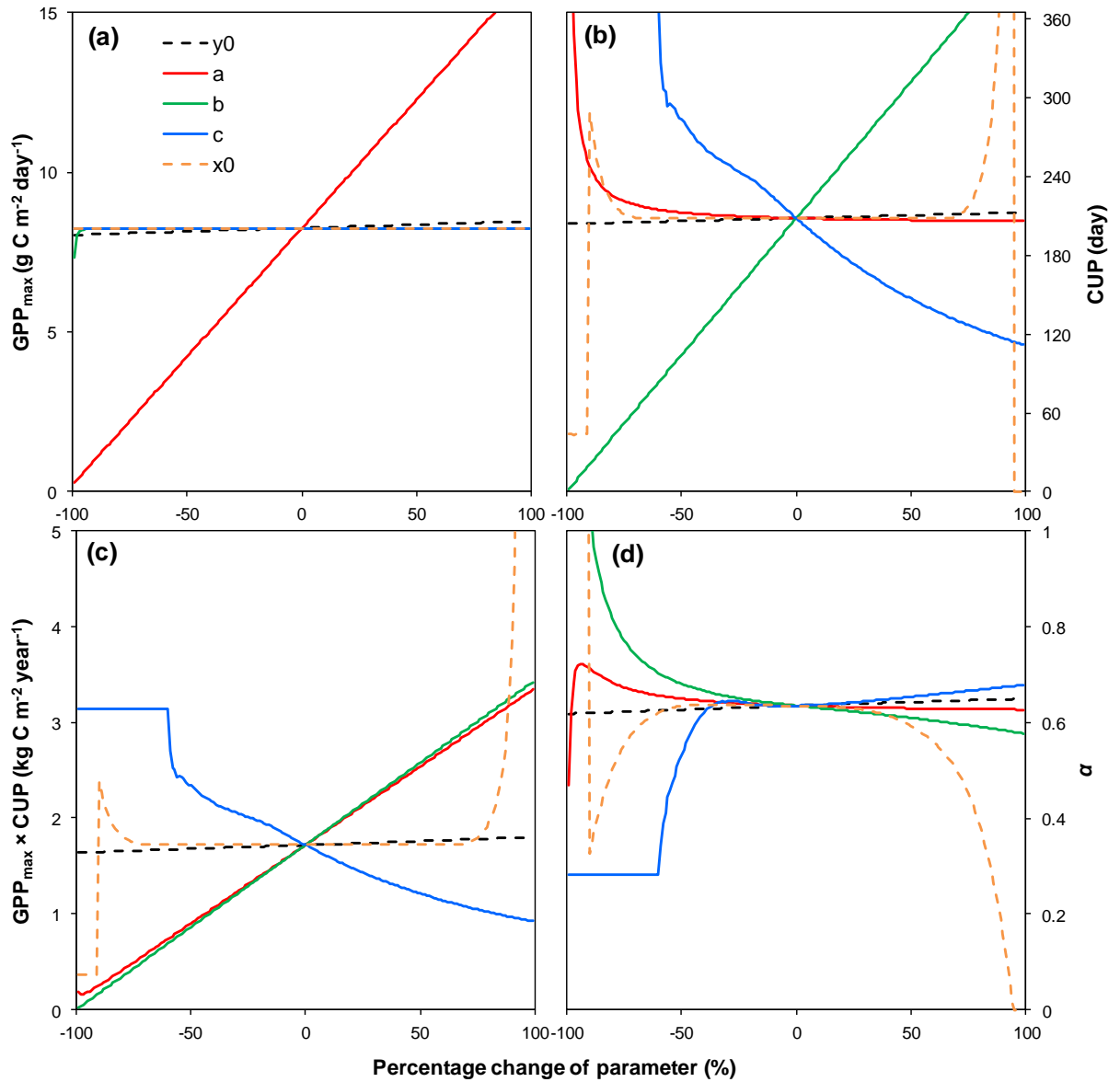
425 Similar to the equations (12) – (13), the maximal (R_{\max}) and minimal (R_{\min}) change rate of
 426 daily GPP are obtained by:

$$427 \quad R_{\max} = \max \{P(t)\} \quad (26)$$

$$428 \quad R_{\min} = \min \{P(t)\} \quad (27)$$

429 The CUP_{start} and CUP_{end} can be calculated by the equations (14) and (15), respectively. The
 430 CUP can be calculated as CUP_{end} minus CUP_{start} , and GPP_{\max} as $\max\{P(t)\}$.

431 In the analysis, we first calculated the bootstrapping medians of all parameters from their
 432 estimations from the eddy-flux sites. Then, we increased each parameter from -100% to
 433 100%, with an interval of 1%, of its calculated medians with other parameters kept at the
 434 estimated values from observations. Finally, we calculated CUP, GPP_{\max} , $CUP \times GPP_{\max}$ and
 435 α with each combination of parameters and plotted their dependences on each parameter in
 436 Fig. S1.6.1. The sensitivity analysis showed that GPP_{\max} is very sensitive to the parameter a
 437 (Fig. S1.6.1a) of the Weibull function, while CUP is mainly affected by the parameters b and
 438 c (Fig. S1.6.1b). The parameters a , b and c together control the variations of the product of
 439 GPP_{\max} and CUP (Fig. S1.6.1c). The ratio between annual GPP and the product of GPP_{\max}
 440 and CUP (α) can be affected by each of the parameters (a , b , c , x_0 , and y_0 ; Fig. S1.6.1d). It
 441 suggests the convergence of α is not the mathematical certainty the of the Weibull function
 442 used in this study.

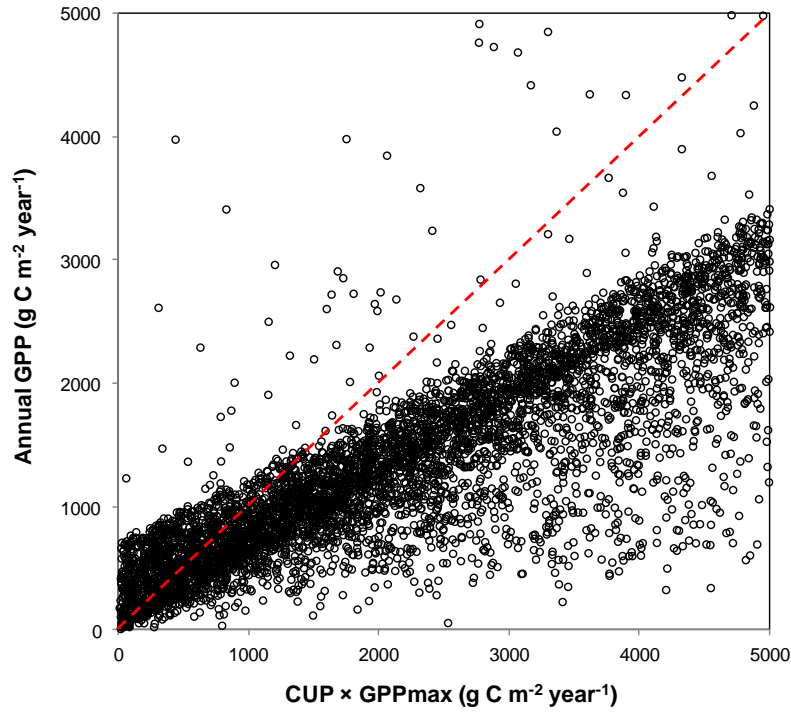


Supplementary Fig. S1.6.1. Sensitivity analyses of parameters. The results are obtained through the following steps: (1) calculate the bootstrapping median of the parameters from the global analyses on flux data; (2) change those parameters from -100% to +100% and calculate the values of GPP_{max} , CUP, $GPP_{max} \times CUP$, and α (annual GPP/($GPP_{max} \times CUP$)) with equations (23) – (25).

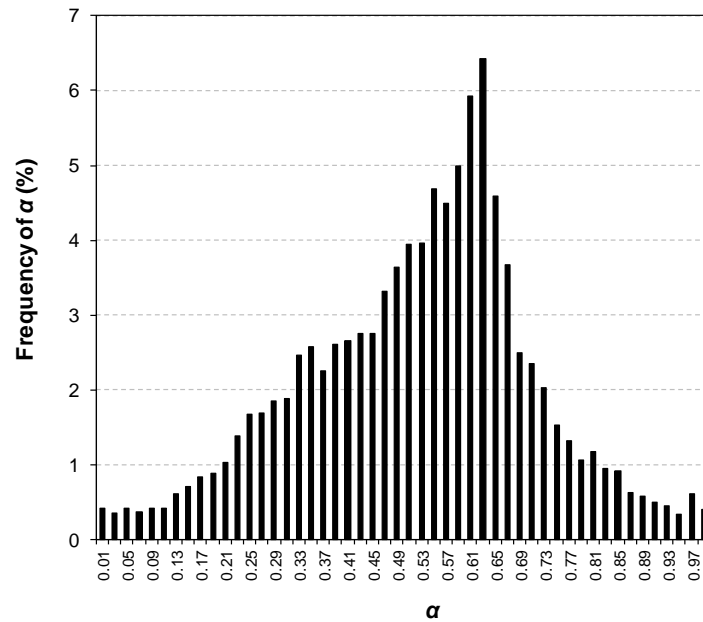
S1.7 Random re-sampling test of the Weibull function

451 We further did a random re-sampling test for the performance of the Weibull function itself in
 452 affecting the ratio between annual GPP and the product of CUP and $GPP_{max}(\alpha)$. The test
 453 consisted of three steps: First, we set up the ranges of each parameter (a , b , c , x_0 , and y_0) in
 454 equation 7, with $0 < a \leq 30$, $0 < b \leq 500$, $1 < c \leq 5$, $0 < x_0 \leq 300$, $0 < y_0 \leq 2$. For each
 455 parameter, the given range covered $> 90\%$ of the estimated values from all FLUXNET sites.
 456 Second, we equally separated the range of each parameter into 10000 samples from the
 457 lowest to largest value. For example, there were 1000 samples of parameter a including
 458 0.003, 0.006, ... , 30. In the third step, we randomly chose each parameter from its 10000
 459 samples to obtain the CUP, GPP_{max} , and annual GPP and thus the α . The random resampling
 460 of parameters was repeated by 2000 times, and the output was used for the further analyses.

461 As shown by Fig. S1.7.1, annual GPP is positively related to the product of CUP and
 462 GPP_{max} . However, the ratio (α) between them diverges. By plotting the frequency distribution
 463 of α that ranges from 0 to 1, we found it follows the normal distribution ($R^2 = 0.85$, $P <$
 464 0.001 ; Fig. S1.7.2). Since the ranges of parameters are chosen based on the estimates in the
 465 natural ecosystems, the highest frequency of α in random resampling test is close to that
 466 found in the original analysis (as shown in Fig. 1 of the main text). However the divergence
 467 of α suggests that the global convergence of α should be caused by ecological processes in
 468 the natural ecosystems, but not the Weibull function itself.



Supplementary Fig. S1.7.1. Results of a random re-sampling test. The parameter ranges were defined according to their distributions in the FLUXNET sites. The red dashed line is the 1:1 line.

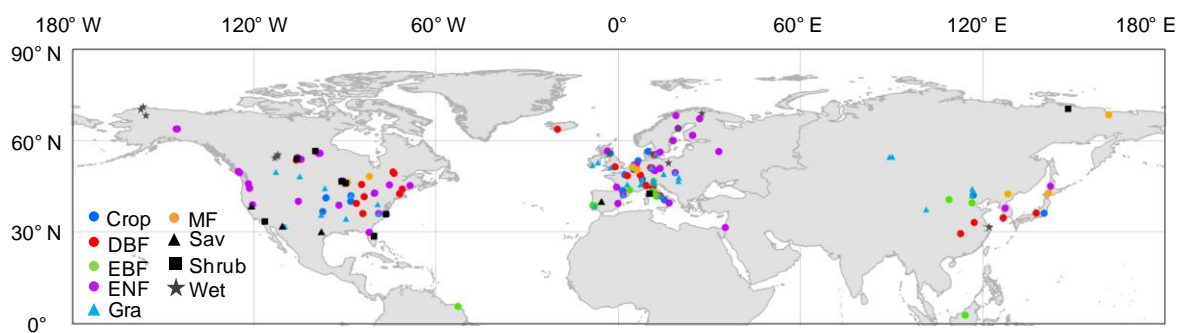


Supplementary Fig. S1.7.2. Frequency of α in the output of the random re-sampling test.

S1.8 Freeze/Thaw Data

Global daily records of landscape freeze/thaw data from 1st January 2000 to 31st December 2010 were analyzed for an additional indicator of CUP. The data were obtained from the NSIDC (<http://nsidc.org/data/nsidc-0477>). More detailed information about the data were provided at: <http://nsidc.org/data/docs/measures/nsidc-0477/index.html>. We used the combined freeze/thaw data (specifically, AM and PM thawed ground-state) to estimate dates of spring thaw and autumn freeze with the approach introduced by some earlier studies (24-26). The spring thaw data was defined as the date corresponding to the 8th day of the first 15 day period in a year when 80% days (i.e., 12 days) is classified as non-frozen days. The similar 80% rule was applied for determine the date of autumn freeze (i.e., end of CUP) for each grid. The global distribution of obtained CUP from the Freeze/Thaw (F/T) data was shown in Fig. S10.

S1.9 Distribution of FLUXNET Sites



Supplementary Fig. S1.9.1. Distribution of FLUXNET sites that used in this study. Crop, cropland; DBF, deciduous broadleaf forest; EBF, evergreen broadleaf forest; ENF, evergreen needleleaf forest; MF, mixed forest; Gra, grassland, Sav, savanna; Shrub, shrubland; Wet, wetland.

As shown in Fig. S1.9.1, the eddy covariance sites are not homogeneously distributed over the global. More sites are distributed in North America, West Europe, and East Asia. Although the FLUXNET sites cannot fully represent the global heterogeneity in environmental conditions, they occupy almost all vegetation types and climate zones in terrestrial ecosystem (Please see more details in the Supporting Online Material of Beer et al.(5)). Our goal in this study is to test the control of phenological and physiological aspects on terrestrial annual GPP, so the broadly distributed FLUXNET sites are plenty to represent most vegetation and climate types in terrestrial ecosystems.

S2. Supplementary Tables and Figures

Table S1. Information of FLUXNET sites used in this study.

Site Name	PFT	Lat	Lon	Year	Ref.
AT-Neu	Grassland	47.1	11.3	2002-2006	(27)
BE-Bra	MF	51.3	4.5	1997-1998,2000-2002,2004-2006	(28)
BE-Lon	Cropland	50.6	4.7	2004-2006	(29)
BE-Vie	MF	50.3	6.0	1997-2006	(30)
BR-Sa1	EBF	-2.85	-54.97	2001-2003	(31)
BR-Sa3	EBF	-3.02	-54.97	2001-2003	(32)
BR-Sp1	Savanna	-21.6	-47.7	2001	(33)
CA-Ca1	ENF	49.9	-125.3	1998-2005	(34)
CA-Ca2	ENF	49.9	-125.3	2001-2005	(34)
CA-Ca3	ENF	49.5	-124.9	2002-2005	(34)
CA-Gro	MF	48.2	-82.2	2004	(35)
CA-Let	Grassland	49.7	-112.9	1999-2005	(36)
CA-Man	ENF	55.9	-98.5	1995,1998-2000	(37)
CA-Mer	ENF	45.4	-75.5	1999-2005	(38)
CA-NS1	ENF	55.9	-98.5	2003-2005	(39)
CA-NS2	ENF	55.9	-98.5	2002-2005	(39)
CA-NS3	ENF	55.9	-98.4	2002-2005	(39)
CA-NS4	ENF	55.9	-98.4	2003-2004	(39)
CA-NS5	ENF	55.9	-98.5	2002-2005	(39)
CA-NS6	ENF	55.9	-99.0	2002-2005	(39)
CA-NS7	Shrubland	56.6	-99.9	2003-2005	(39)

CA-Oas	DBF	53.6	-106.2	1997-2005	(40)
CA-Ojp	DBF	53.9	-104.7	2000-2003,2005	(41)
CA-Qcu	DBF	49.3	-74.0	2002-2006	(42)
CA-Qfo	DBF	49.7	-74.3	2004-2006	(43)
CA-SF1	ENF	54.5	-105.8	2004	(44)
CA-SF2	ENF	54.3	-105.9	2003-2004	(44)
CA-SF3	Shrubland	54.1	-106.0	2003-2005	(44)
CA-SJ1	ENF	53.9	-104.7	2001-2005	(45)
CA-SJ2	ENF	53.9	-104.6	2003-2005	(45)
CA-SJ3	ENF	53.9	-104.6	2004-2005	(45)
CA-TP1	ENF	42.7	-80.6	2004-2005	(46)
CA-TP2	ENF	42.8	-80.5	2004-2005	(46)
CA-TP3	ENF	42.7	-80.3	2005	(46)
CA-TP4	ENF	42.7	-80.4	2004-2005	(47)
CA-WP1	Wetland	55.0	-112.5	2004-2005	(48)
CA-WP2	Wetland	55.5	-112.3	2004	(49)
CA-WP3	Wetland	54.5	-113.3	2004	(49)
CH-Oe1	Grassland	47.3	7.7	2002-2006	(50)
CH-Oe2	Cropland	47.3	7.7	2005	(51)
CN-Anh	DBF	33.0	117.0	2005-2006	(52)
CN-Bed	EBF	39.5	116.3	2005	(52)
CN-Cha	MF	42.4	128.1	2003	(53)
CN-Do1	Wetland	31.5	122.0	2005	(54)
CN-Do2	Wetland	31.6	121.9	2005	(54)
CN-Do3	Wetland	31.5	122.0	2005	(54)
CN-Du1.	Cropland	42.0	116.7	2005-2006	(55)
CN-Du2	Grassland	42.0	116.3	2006	(55)
CN-HaM	Grassland	37.4	101.2	2002-2003	(56)
CN-Hny	DBF	29.3	112.5	2005-2006	-
CN-Ku1	EBF	40.5	108.7	2006	(57)
CN-Xfs	Grassland	44.1	116.3	2004-205	-
CZ-BK1	ENF	49.5	18.5	2001,2004-2006	-
CZ-BK2	Grassland	49.5	18.5	2005-2006	-
CZ-wet	Grassland	49.0	14.8	2006	(58)
DE-Bay	ENF	50.1	11.9	1997-1999	(59)
DE-Geb	Cropland	51.1	10.9	2004-2006	(60)
DE-Gri	Cropland	50.9	13.5	2005-2006	(16)
DE-Hai	DBF	51.1	10.5	2000-2006	(61)
DE-Har	DBF	51.1	10.5	2005-2006	(62)
DE-Kli	Cropland	50.9	13.5	2005-2006	-
DE-Meh	Grassland	51.3	10.7	2004-2006	(63)
DE-Tha	ENF	51.0	13.6	1997-2006	(64)
DE-Wet	ENF	50.5	11.5	2002-2006	(65)
DK-Fou	Cropland	56.5	9.6	2005	-
DK-Lva	Grassland	55.7	12.1	2005-2006	(16)

DK-Ris	Cropland	55.5	12.1	2004-2005	(66)
DK-Sor	DBF	55.5	11.6	1996-2006	(66)
ES-ES1	ENF	39.3	-0.3	1999-2002,2004-2006	(3)
ES-ES2	Cropland	39.3	-0.3	2004-2006	–
ES-LMa	Savanna	39.9	-5.8	2004-2006	(67)
ES-VDA	Grassland	42.2	1.4	2004-2005	(61)
FI-Hyy	ENF	61.8	24.3	1997-2006	(68)
FI-Kaa	Wetland	69.1	27.3	2000-2006	(69)
FI-Sii	ENF	61.8	24.2	2004-2005	(70)
FI-Sod	ENF	67.4	26.6	2000-2006	(71)
FR-Aur	Cropland	43.5	1.1	2005	–
FR-Fon	DBF	48.5	2.8	2005-2006	–
FR-Gri	Cropland	48.8	2.0	2005-2006	(72)
FR-Hes	DBF	48.7	7.1	1997-2006	(73)
FR-Lam	Cropland	43.5	1.2	2005	–
				1997-1998,2000,2004-2006	(74)
FR-LBr	ENF	44.7	-0.8		
FR-Lq1	Grassland	45.6	2.7	2004-2006	(16)
FR-Lq2	Grassland	45.6	2.7	2004-2006	(16)
FR-Pue	EBF	43.7	3.6	2001-2006	(75)
GF-Guy	EBF	5.3	-52.9	2005-2006	(76)
HU-Bug	Grassland	46.7	19.6	2003-2006	(77)
HU-Mat	Grassland	47.8	19.7	2004-2006	(78)
ID-Pag	EBF	2.3	114.0	2002-2003	(79)
IE-Ca1	Grassland	52.9	-6.9	2004-2006	–
IE-Dri	Grassland	52.0	-8.8	2003-2004	(80)
IL-Yat	ENF	31.3	35.1	2001-2006	(21)
IS-Gun	DBF	63.8	-20.2	1997-1998	(81)
IT-Amp	Grassland	41.9	13.6	2003-2006	(16)
IT-BCi	Cropland	40.5	15.0	2004-2006	(82)
IT-Bon	ENF	39.5	16.5	2006	–
IT-Col	DBF	41.8	13.6	1997-2005	(83)
IT-Cpz	EBF	41.7	12.4	1997,2001,2003-2006	(84)
IT-Lav	ENF	39.5	16.5	2001-2002,2004,2006	(85)
IT-Lec	EBF	43.3	11.3	2006	–
IT-LMa	Grassland	45.6	7.2	2003-2005	–
IT-Mal	Grassland	46.1	11.7	2003	–
IT-MBo	Grassland	46.0	11.0	2003-2006	(86)
IT-Non	DBF	44.7	11.1	2001-2003,2006	–
IT-Pia	Shrubland	42.6	10.1	2002-2005	(87)
IT-PT1	DBF	45.2	9.1	2002-2004	(88)
IT-Ren	EBF	46.6	11.4	1999,2001-2006	(89)
IT-Ro1	DBF	42.4	11.9	2001-2006	(90)
IT-Ro2	DBF	42.4	11.9	2002-2006	(91)
IT-SRo	ENF	39.5	16.5	1999-2006	(92)

IT-Vig	DBF	45.3	8.9	2005	–
JP-Mas	Cropland	36.1	140.0	2002-2003	(93)
JP-Tak	DBF	36.1	137.4	1999-2004	(94)
JP-Tef	ENF	45.1	142.1	2002,2004-2005	(95)
JP-Tom	MF	42.7	141.5	2001-2003	(96)
KR-Hnm	DBF	34.6	126.6	2004-2006	(97)
KR-Kw1	ENF	37.7	127.2	2005-2006	(98)
NL-Ca1	Grassland	52.0	4.9	2003-2006	(99)
NL-Hor	Grassland	52.0	5.1	2005-2006	(99)
NL-Lan	Cropland	52.0	4.9	2005	(99)
NL-Loo	ENF	52.2	5.7	1997-2006	(100)
NL-Lut	Cropland	53.4	6.4	2006	(101)
NL-Mol	Cropland	51.7	4.6	2005	(101)
PL-wet	Wetland	52.8	16.3	2004-2005	(102)
PT-Esp	EBF	38.6	-8.6	2002-2004,2006	(103)
PT-Mi1	EBF	38.5	-8.0	2003-2005	(104)
PT-Mi2	Grassland	38.5	-8.0	2006	(104)
RU-Che	MF	68.6	161.3	2003-2004	(105)
RU-Cok	Shrubland	70.6	147.9	2003	(106)
RU-Fyo	ENF	56.5	32.9	1998-2006	(107)
RU-Ha1	Grassland	54.7	90.0	2003-2004	(108)
RU-Ha3	Grassland	54.7	89.1	2004	(108)
RU-Zot	ENF	56.5	32.9	2002-2004	–
SE-Abi	ENF	68.4	18.8	2005	–
SE-Deg	Wetland	64.2	19.6	2001-2005	(109)
SE-Faj	ENF	56.3	13.6	2006	(110)
SE-Fla	ENF	64.1	19.5	1997-1998	(111)
SE-Fla	ENF	64.1	19.5	2001-2002	(111)
SE-Nor	EBF	60.1	17.5	1996-1999,2003	(112)
SE-Sk1	ENF	60.1	17.9	2005	–
SE-Sk2	ENF	60.1	17.8	2004-2005	–
UK-AMo	Wetland	55.8	-3.2	2005	(113)
UK-EBu	Grassland	55.9	-3.2	2004-2006	(114)
UK-ESa	Cropland	55.9	-2.9	2004-2005	–
				1997-1998,2000-2001,2005-2006	(115)
UK-Gri	ENF	56.6	-3.8		
UK-Ham	DBF	34.6	126.6	2004-2005	(116)
UK-PL3	DBF	51.5	-1.3	2005	–
UK-Tad	Grassland	51.2	-2.8	2001	(117)
US-ARb	Grassland	35.5	-98.0	2005-2006	–
US-ARc	Grassland	35.5	-98.0	2005-2006	–
US-ARM	Cropland	36.6	-97.5	2003-2006	(17)
US-Atq	Wetland	70.5	-157.4	2001,2003,2005-2006	(118)
US-Aud	Grassland	31.6	-110.5	2002,2005-2006	–
US-Bar	DBF	44.1	-71.3	2004-2005	(119)

US-Bkg	Grassland	44.3	-96.8	2005-2006	(120)
US-Blo	ENF	38.9	-120.6	2000-2006	(121)
US-Bn1	ENF	63.9	-145.4	2003	(122)
US-Bn2	ENF	63.9	-145.4	2003	(122)
US-Bn3	ENF	63.9	-145.7	2003	(122)
US-Bo1	Cropland	40.0	-88.3	1997-2006	(123)
US-Bo2	Cropland	40.0	-88.3	2004-2006	(123)
US-Brw	Wetland	71.3	-156.6	19,982,001	(124)
US-CaV	Grassland	39.1	-79.4	2004	–
US-Dk1	Grassland	36.0	-79.1	2002-2005	(125)
US-Dk2	DBF	36.0	-79.1	2003-2005	(125)
US-Dk3	ENF	36.0	-79.1	2001-2005	(125)
US-FPe	Grassland	48.3	-105.1	2000-2006	–
US-FR2	Savanna	29.9	-98.0	2004-2006	(126)
US-Goo	Grassland	34.3	-89.9	2002-2006	–
US-Ha1	DBF	42.5	-72.2	1992-2006	(127)
US-Ho1	ENF	45.2	-68.7	1996-2004	(128)
US-Ho2	ENF	45.2	-68.7	1999-2004	(128)
US-IB1	Cropland	41.9	-88.2	2006-2007	(129)
US-IB2	Grassland	41.8	-88.2	2006-2007	(129)
US-Ivo	Wetland	68.5	-155.8	2004-2006	–
US-KS2	Shrubland	28.6	-80.7	2001-2002,2004-2006	(130)
US-Los	Shrubland	46.1	-90.0	2001-2003,2005	–
US-LPH	DBF	42.5	-72.2	2003-2004	(131)
US-Me2	ENF	44.5	-121.6	2003-2005	(132)
US-Me3	ENF	44.3	-121.6	2004-2005	(132)
US-Me4	ENF	44.5	-121.6	1996-1997,2000	(132)
US-MMS	DBF	39.3	-86.4	1999-2005	(133)
US-NC1	Shrubland	35.8	-76.7	2005-2006	(134)
US-NC2	ENF	35.8	-76.7	2005-2006	(135)
US-Ne1	Cropland	41.2	-96.5	2001-2004	(136)
US-Ne2	Cropland	41.2	-96.5	2003-2004	(136)
US-Ne3	Cropland	41.2	-96.4	2001-2004	(136)
US-NR1	ENF	40.0	-105.5	1999-2000,2002-2003	(137)
US-Oho	DBF	41.6	-83.8	2004-2005	(138)
US-PFa	MF	45.9	-90.3	1997-2000,2003	(139)
US-SO2	Shrubland	33.4	-116.6	2004-2006	(140)
US-SO3	Shrubland	33.4	-116.6	20,012,005	(140)
US-SO4	Shrubland	33.4	-116.6	2005-2006	–
US-SP1	ENF	29.7	-82.2	2005	(141)
US-SP2	ENF	29.8	-82.2	1999-2004	(142)
US-SP3	ENF	29.8	-82.2	1999,2001-2004	(142)
US-SRM	Savanna	31.8	-110.9	2004-2006	(143)
US-Syv	MF	46.2	-89.3	2002-2006	(144)
US-Ton	Savanna	38.4	-121.0	2002-2006	(145)

US-UMB	DBF	45.6	-84.7	1999-2003	(146)
US-WBW	DBF	36.0	-84.3	1995-1999	(147)
US-WCr	DBF	45.8	-90.1	1999-2006	(148)
US-Wi0	ENF	46.6	-91.1	2002	(149)
US-Wi1	DBF	46.7	-91.2	2003	(150)
US-Wi2	ENF	46.7	-91.2	2003	(150)
US-Wi4	ENF	46.7	-91.2	2002-2005	(150)
US-Wi5	ENF	46.7	-91.1	2004	(150)
US-Wi6	Shrubland	46.6	-91.3	2002	(150)
US-Wi7	Shrubland	46.6	-91.1	2005	(150)
US-Wi8	DBF	46.7	-91.3	2002	(150)
US-Wkg	Grassland	31.7	-109.9	2005-2006	(151)
US-Wrc	ENF	45.8	-122.0	1999-2002,2004,2006	(152)
VU-Coc	EBF	-15.4	167.2	2002	(153)

509

Table S2. Results of partial correlation analyses for FLUXNET GPP. The dependent variable is annual GPP and independent variables are GPPmax and CUP.

	Variable entered	Parameter estimate	Patial r^2	Probability
All	GPP _{max}	0.98	0.72	<0.001
	CUP	0.96	0.26	<0.001
ENF	GPP _{max}	1.00	0.83	<0.001
	CUP	0.99	0.16	<0.001
DBF	GPP _{max}	1.00	0.87	<0.001
	CUP	0.99	0.11	<0.001
EBF	GPP _{max}	0.95	0.80	<0.001
	CUP	1.13	0.18	<0.001
MF	GPP _{max}	0.96	0.79	0.0014
	CUP	1.01	0.21	<0.001
GRA	GPP _{max}	1.00	0.70	0.005
	CUP	0.90	0.28	<0.001
SHRUB	GPP _{max}	0.90	0.52	0.0053
	CUP	1.06	0.43	<0.001
SAV	GPP _{max}	1.23	0.89	0.0014
	CUP	0.80	0.08	0.020
WET	GPP _{max}	1.02	0.91	<0.001
	CUP	0.82	0.08	0.002
CROP	CUP	0.88	0.58	0.0012
	GPPmax	0.86	0.37	<0.001

Figure S1. Relationship between GPP_{max} and CUP across all FLUXNET site-years in this study.

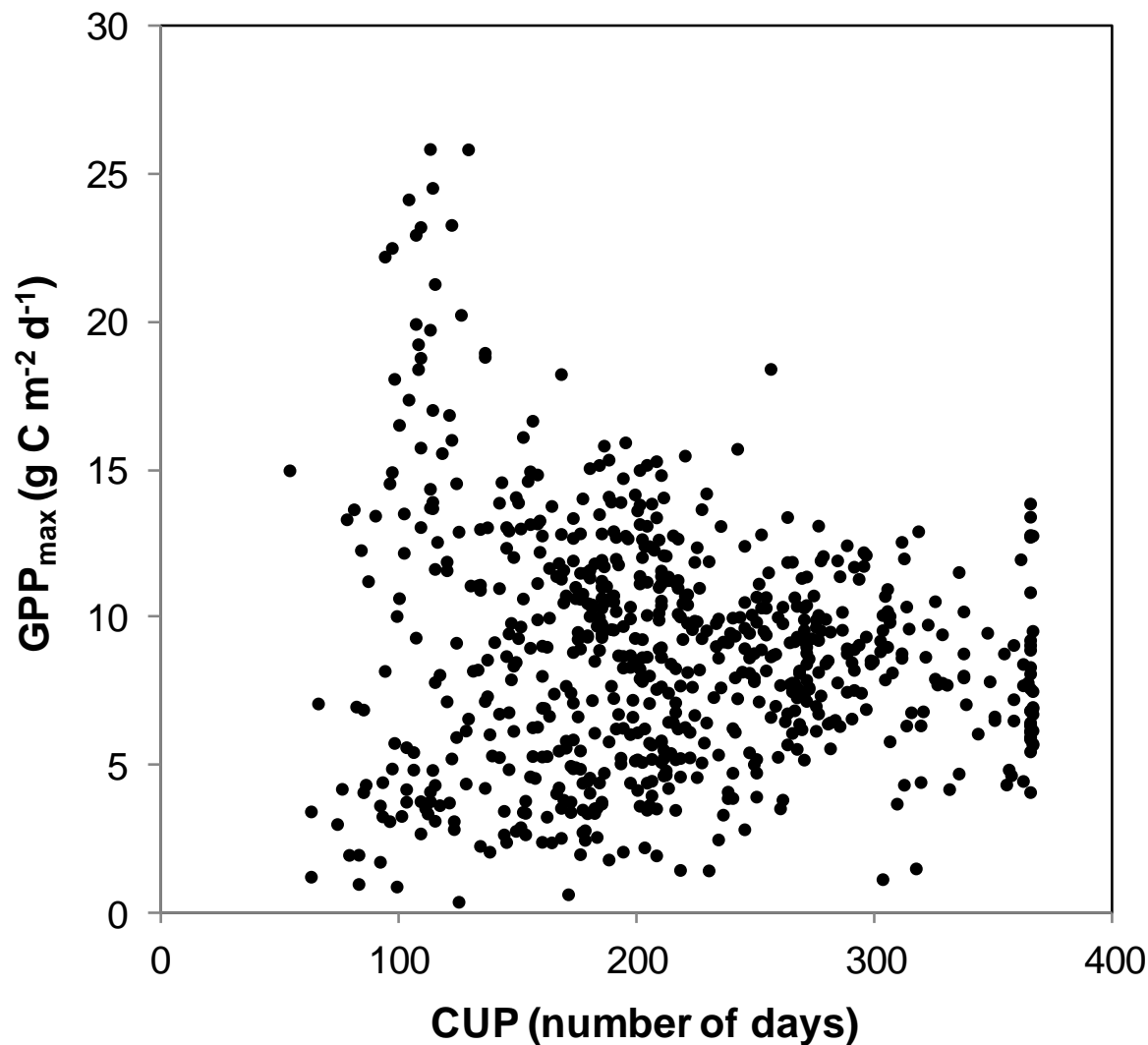


Figure S2. Dynamics of annual GPP, GPP_{max} and CUP from 2000 to 2010 in the Black Hills National Forest, South Dakota, USA. The results were obtained from the MODIS GPP observations in a $0.1 \times 0.1^\circ$ grid pixel ($43.85^\circ N$, $103.95^\circ W$) which is located in the burned area in the Black Hills National Forest. More information about the fire disturbance and the following recovery of vegetation greenness can be found in Xiao *et al.*(154) . The linear regressions of annual GPP, GPP_{max} and CUP against year are all significant (all $P < 0.05$).

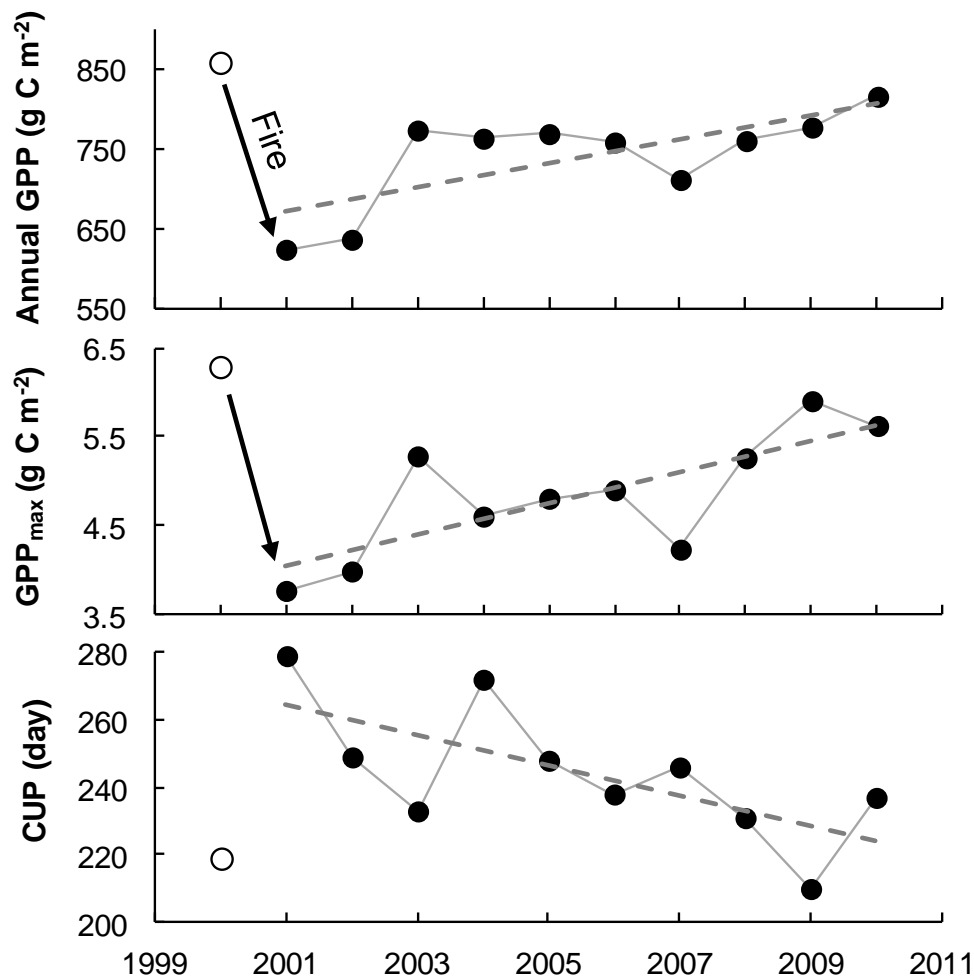


Figure S3. The relative frequency distribution of estimated α from all (a) non-tropical and (b) tropical and subtropical (including Mediterranean climate) FLUXNET site-years.

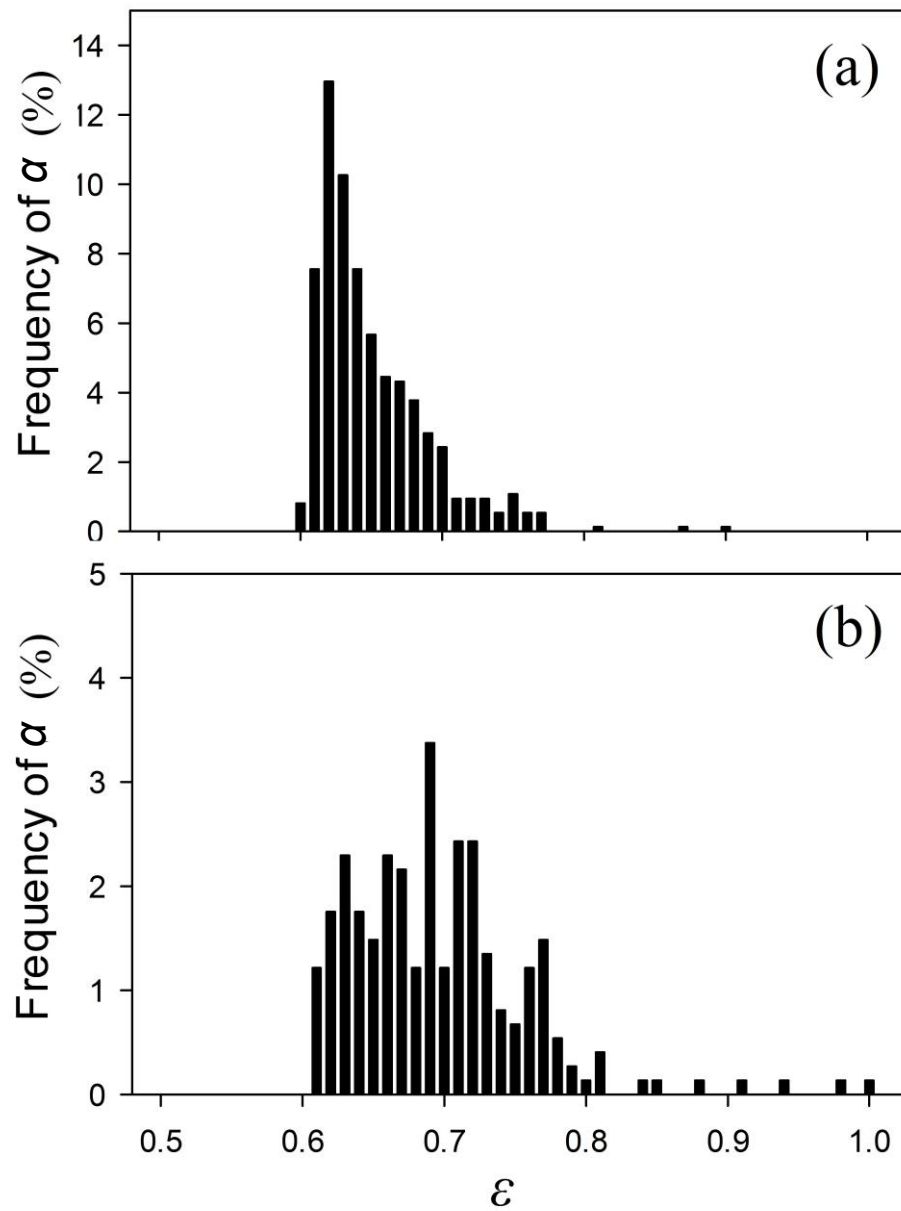


Figure S4. Spatial distributions of mean (a) annual GPP, (b) GPP_{max} , and (c) CUP in North America. Data in each $0.1^\circ \times 0.1^\circ$ grid was averaged over 11 years from 2000 to 2010.

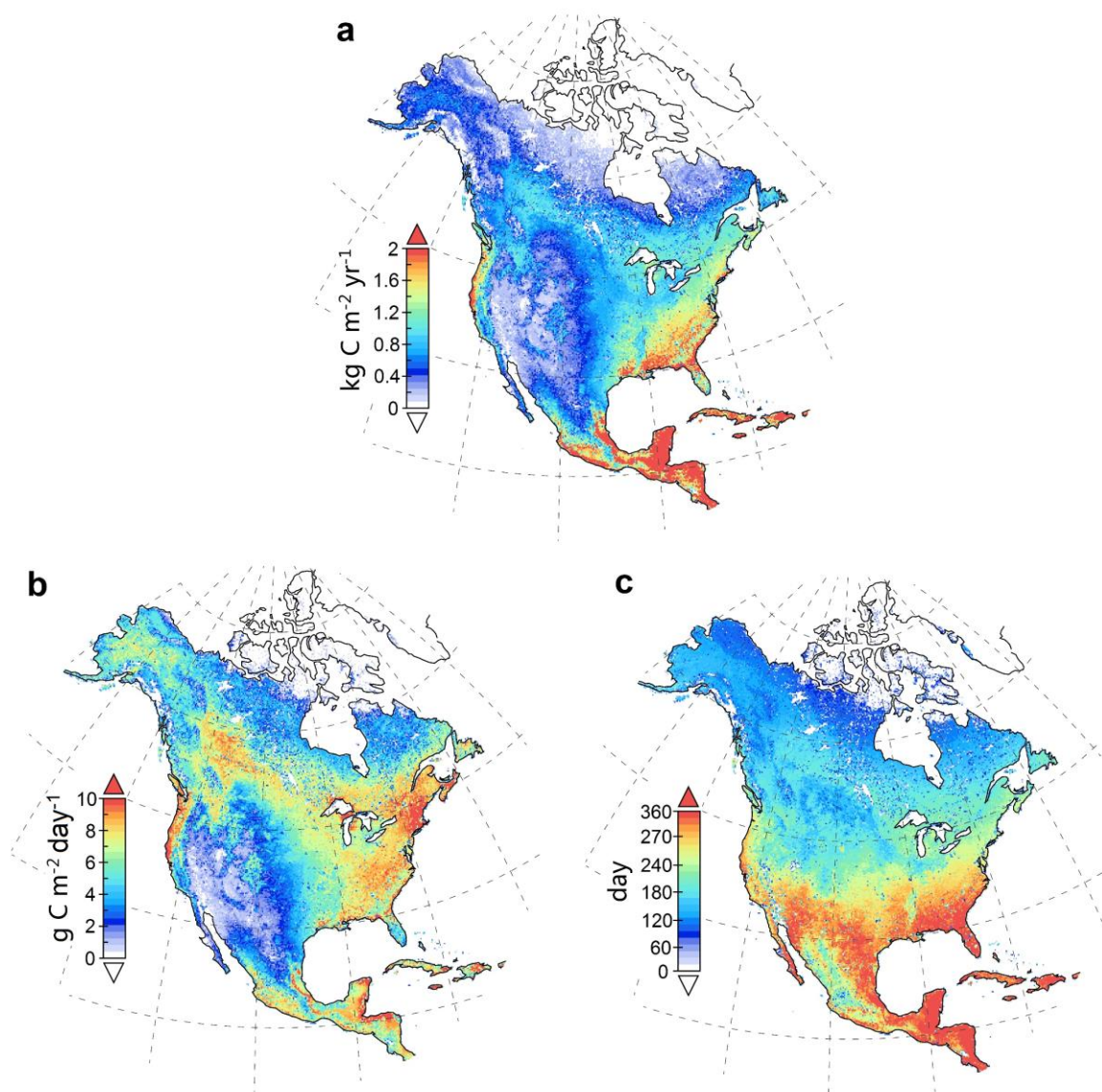


Figure S5. Examples of flux site-year with multiple peaks of daily GPP. Numbers and the associated arrows show the different GPP peaks. The detailed information for each flux site can be found in Table S1.

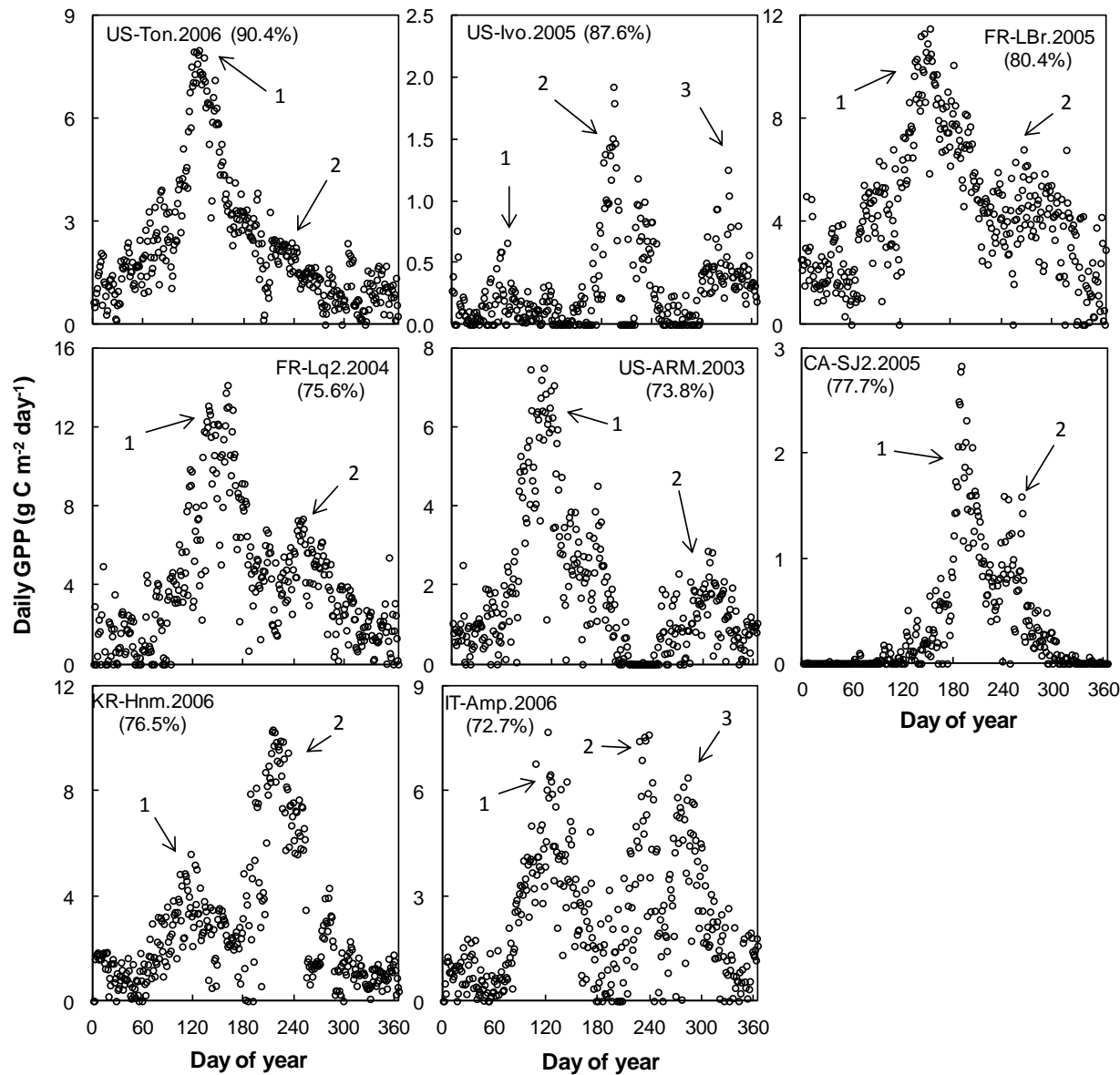


Figure S6. Dependence of annual FLUXNET GPP variability on (a) CUP and (b) GPP_{max} (the linear correlation was tested at the significance level of $P = 0.05$).

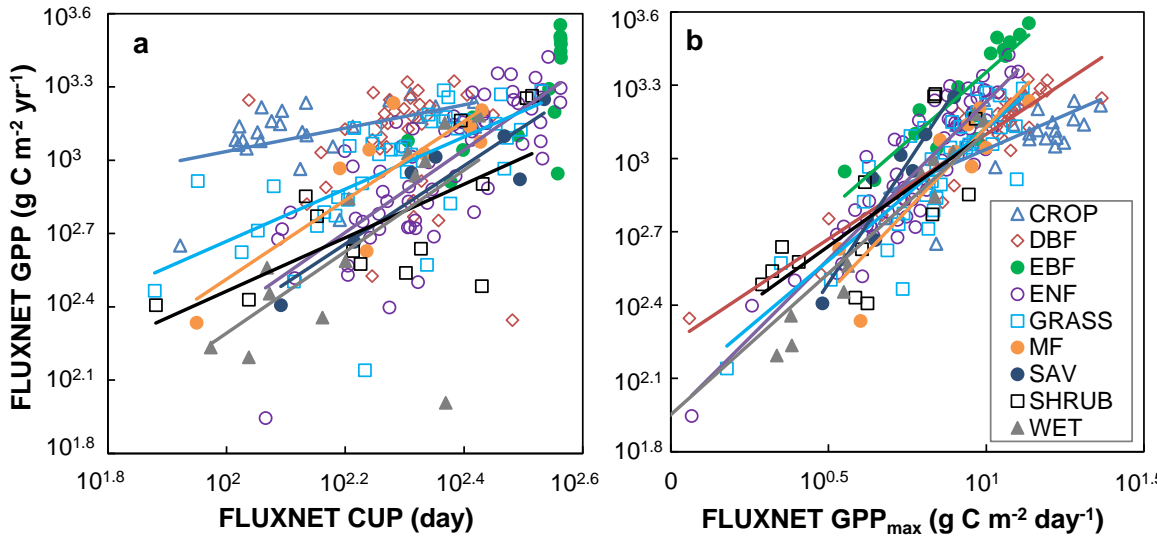


Figure S7. Relationship between MODIS- and FLUXNET-derived GPP_{max} in North America. The MODIS GPP_{max} (0.1 °by 0.1 °degree) from the latitude-longitude grid cell where the flux-tower site located was used for the analysis.

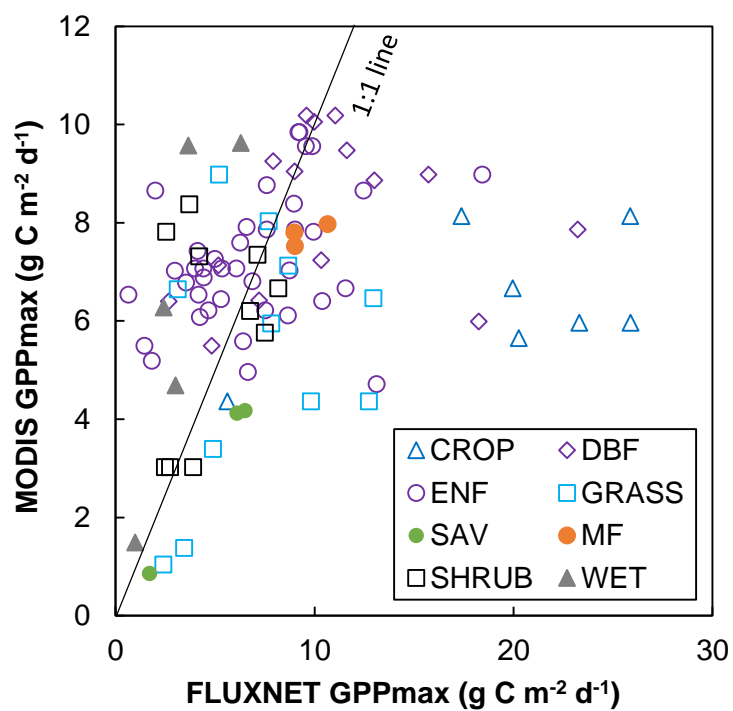


Figure S8. (a) Global distribution of averaged CUP over 2000-2010 derived from the daily records of landscape freeze/thaw (F/T) data with the spatial resolution of 25km by 25km. (b) Comparison between the MODIS- and F/T-derived CUP in North America. More details of the data and method are provided in S1.9. The F/T data were firstly re-gridded into 0.1 ° by 0.1 °, and then both the MODIS- and F/T-derived were averaged along latitude with a 0.5 ° interval.

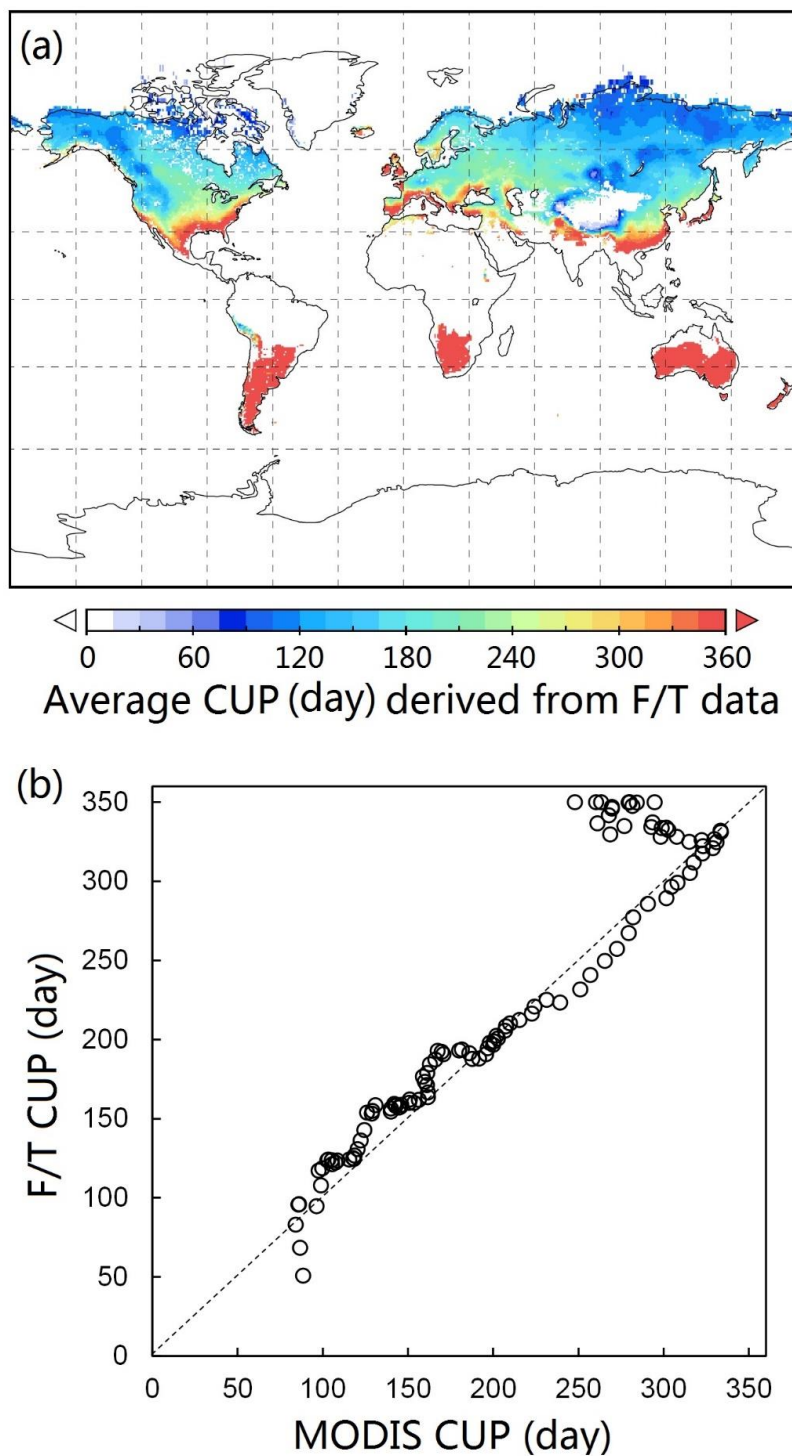


Figure S9. GPP dynamics in 2002 and 2003 at 10 FLUXNET sites in Europe. The year 2003 was extremely hot and dry, with July temperature up to 6 °C above and annual precipitation about 50% below the long-term averages(155). The selection of sites is based on the ref (149), which analyzed the impacts of the 2003 heatwave on European primary productivity. According to that study, GPP in 2002 (black triangle) was chosen as a reference and the impact of 2003 heatwave was calculated as the relative changes in 2003 (red circle) from those in 2002. The site information can be found in Table S1.

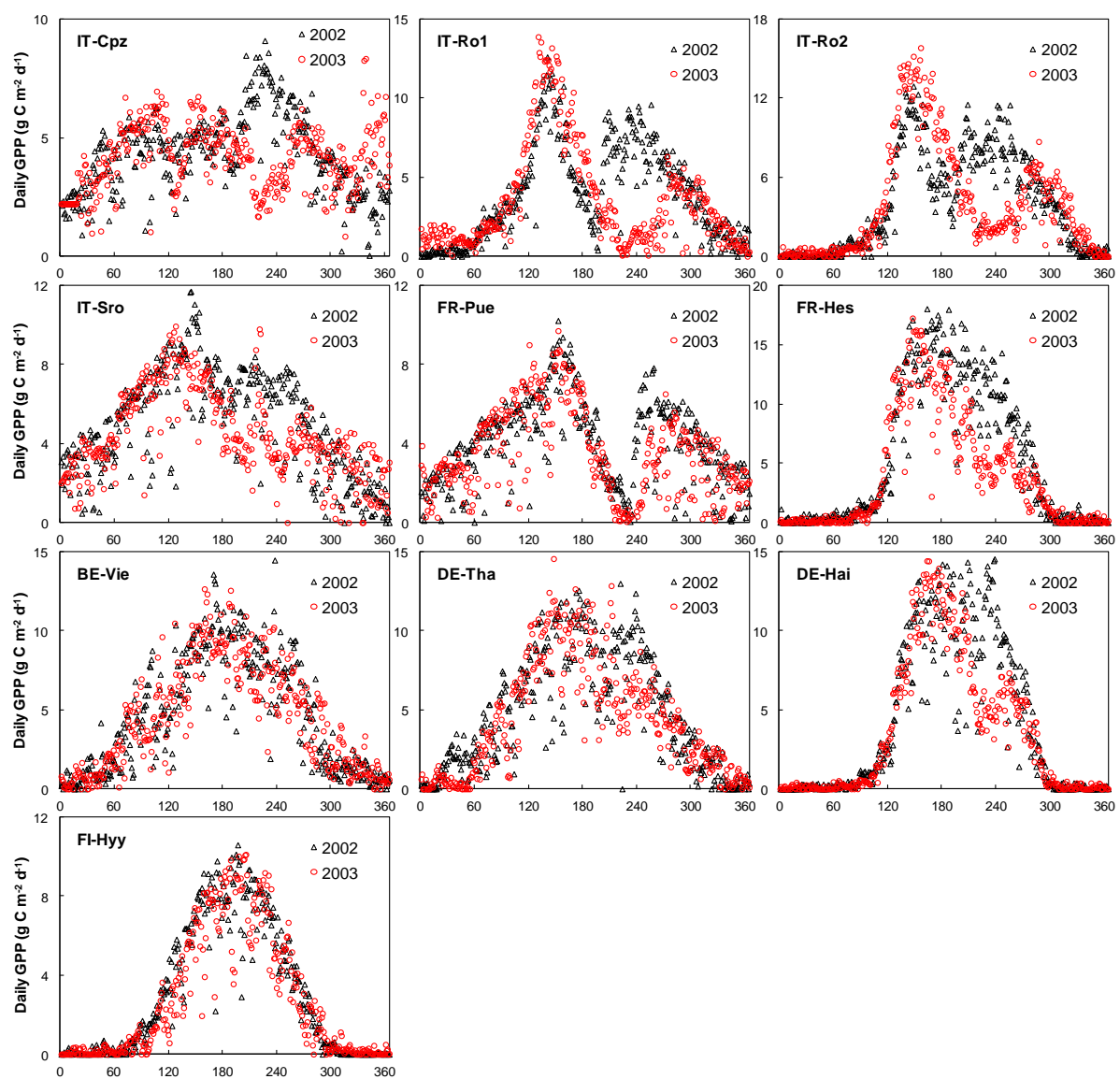
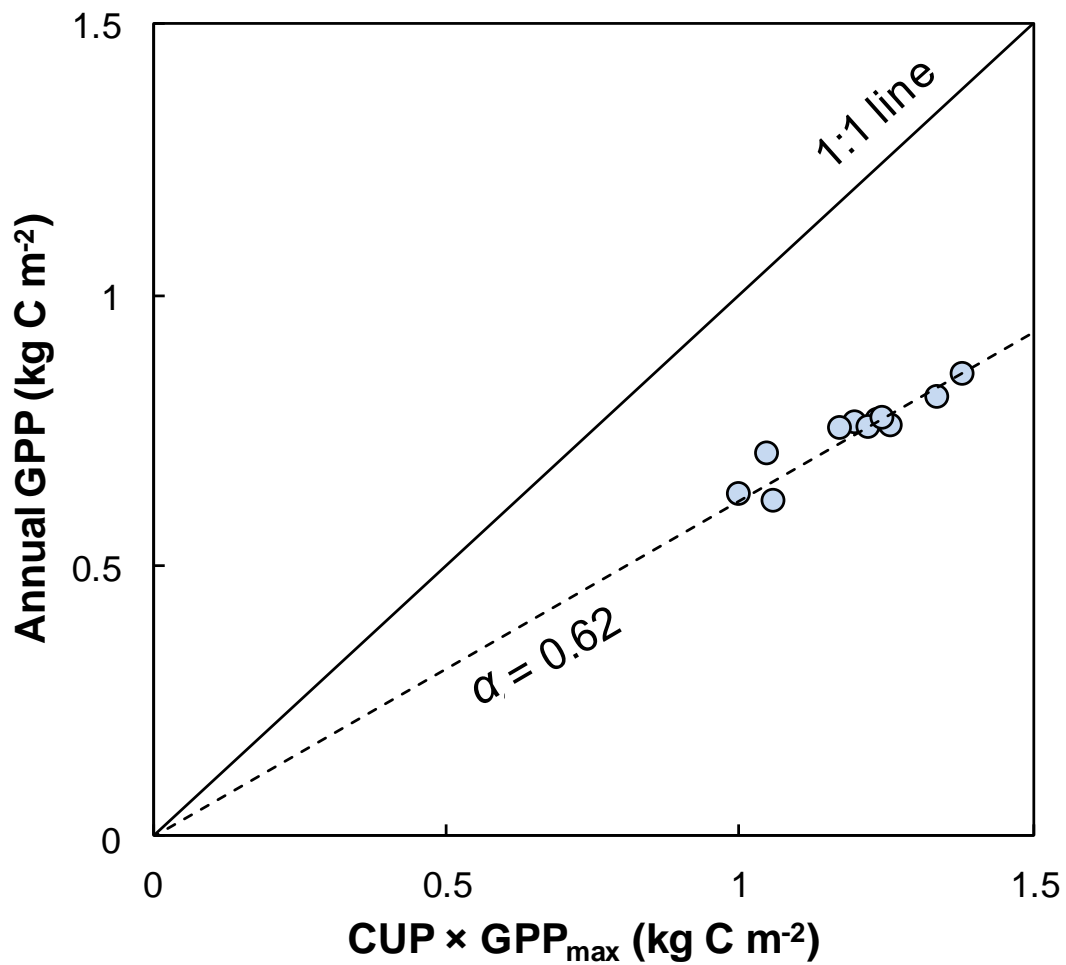


Figure S10. Relationship between annual GPP and the product of CUP and GPP_{max} in the Black Hills National Forest, South Dakota, USA. Each circle represents a year from 2000 to 2010. The results were obtained from the MODIS GPP observations in a $0.1 \times 0.1^\circ$ grid pixel ($43.85^\circ N$, $103.95^\circ W$) which located in the burned area in the Black Hills National Forest. More information about the fire disturbance and the following recovery of vegetation greenness can be found in Xiao *et al.*(154) .



Supporting References

1. Baldocchi D, et al. (2001) FLUXNET: a new tool to study the temporal and spatial variability of ecosystem-scale carbon dioxide, water vapor, and energy flux densities. *Bulletin of the American Meteorological Society* 82(11):2415-2434.
2. Gu L, et al. (2003) Phenology of vegetation photosynthesis. *Phenology: An integrative environmental science*, (Springer), pp 467-485.
3. Reichstein M, et al. (2005) On the separation of net ecosystem exchange into assimilation and ecosystem respiration: review and improved algorithm. *Global Change Biol* 11(9):1424-1439.
4. Papale D, et al. (2006) Towards a standardized processing of Net Ecosystem Exchange measured with eddy covariance technique: algorithms and uncertainty estimation. *Biogeosciences* 3(4):571-583.
5. Beer C, et al. (2010) Terrestrial gross carbon dioxide uptake: global distribution and covariation with climate. *Science* 329(5993):834-838.
6. Moncrieff JB, Malhi Y, & Leuning R (1996) The propagation of errors in long-term measurements of land-atmosphere fluxes of carbon and water. *Global Change Biol* 2(3):231-240.
7. Moffat AM, et al. (2007) Comprehensive comparison of gap-filling techniques for eddy covariance net carbon fluxes. *Agr Forest Meteorol* 147(3-4):209-232.
8. Desai AR, et al. (2008) Cross-site evaluation of eddy covariance GPP and RE decomposition techniques. *Agr Forest Meteorol* 148(6-7):821-838.
9. Heinsch FA, et al. (2003) GPP and NPP (MOD17A2/A3) Products NASA MODIS Land Algorithm. *MOD17 User's Guide*:1-57.
10. Zhao MS, Heinsch FA, Nemani RR, & Running SW (2005) Improvements of the MODIS terrestrial gross and net primary production global data set. *Remote Sens Environ* 95(2):164-176.
11. Zhao MS & Running SW (2010) Drought-induced reduction in global terrestrial net primary production from 2000 Through 2009. *Science* 329(5994):940-943.
12. Running SW, et al. (2004) A continuous satellite-derived measure of global terrestrial primary production. *Bioscience* 54(6):547-560.
13. Sjöström M, et al. (2011) Exploring the potential of MODIS EVI for modeling gross primary production across African ecosystems. *Remote Sens Environ* 115(4):1081-1089.
14. Gu L, et al. (2009) Characterizing the seasonal dynamics of plant community photosynthesis across a range of vegetation types. *Phenology of Ecosystem Processes*, (Springer), pp 35-58.
15. Jönsson P & Eklundh L (2004) TIMESAT—a program for analyzing time-series of satellite sensor data. *Computers & Geosciences* 30(8):833-845.
16. Gilmanov TG, et al. (2007) Partitioning European grassland net ecosystem CO₂ exchange into gross primary productivity and ecosystem respiration using light response function analysis. *Agr Ecosyst Environ* 121(1-2):93-120.

17. Fischer ML, Billesbach DP, Berry JA, Riley WJ, & Torn MS (2007) Spatiotemporal variations in growing season exchanges of CO₂, H₂O, and sensible heat in agricultural fields of the Southern Great Plains. *Earth Interact* 11, 10.1175/EI231.1
18. Liu XJ, Ju XT, Zhang FS, Pan JR, & Christie P (2003) Nitrogen dynamics and budgets in a winter wheat-maize cropping system in the North China Plain. *Field Crop Res* 83(2):111-124.
19. Eklundha L & Jönssonb P (2012) Timesat 3.1 Software Manual.
20. Giorgi F & Lionello P (2008) Climate change projections for the Mediterranean region. *Global Planet Change* 63(2-3):90-104.
21. Grunzweig JM, Lin T, Rotenberg E, Schwartz A, & Yakir D (2003) Carbon sequestration in arid-land forest. *Global Change Biol* 9(5):791-799.
22. Bates DM & Watts DG (1988) Nonlinear regression: iterative estimation and linear approximations (Wiley Online Library).
23. Fox J (2002) Nonlinear regression and nonlinear least squares. appendix to an R and S-PLUS companion to applied regression. (Sage Publications, Ca).
24. Xu L, et al. (2013) Temperature and vegetation seasonality diminishment over northern lands. *Nature Climate Change* 3(6):581-586.
25. Kim Y, Kimball JS, Zhang K, & McDonald KC (2012) Satellite detection of increasing Northern Hemisphere non-frozen seasons from 1979 to 2008: Implications for regional vegetation growth. *Remote Sens Environ* 121:472-487.
26. Zhang K, Kimball JS, Kim Y, & McDonald KC (2011) Changing freeze-thaw seasons in northern high latitudes and associated influences on evapotranspiration. *Hydrol Process* 25(26):4142-4151.
27. Wohlfahrt G, et al. (2008) Seasonal and inter-annual variability of the net ecosystem CO₂ exchange of a temperate mountain grassland: Effects of weather and management. *J Geophys Res-Atmos* 113, D08110, doi:10.1029/2007JD009286.
28. Carrara A, Janssens IA, Yuste JC, & Ceulemans R (2004) Seasonal changes in photosynthesis, respiration and NEE of a mixed temperate forest. *Agr Forest Meteorol* 126(1-2):15-31.
29. Moureaux C, Debacq A, Bodson B, Heinesch B, & Aubinet M (2006) Annual net ecosystem carbon exchange by a sugar beet crop. *Agr Forest Meteorol* 139(1-2):25-39.
30. Aubinet M, et al. (2001) Long term carbon dioxide exchange above a mixed forest in the Belgian Ardennes. *Agr Forest Meteorol* 108(4):293-315.
31. Tota J, et al. (2008) Amazon rain forest subcanopy flow and the carbon budget: Santarem LBA-ECO site. *J Geophys Res-Bioge* 113, G00B02, doi:10.1029/2007JG000597.
32. Huete AR, et al. (2006) Amazon rainforests green-up with sunlight in dry season. *Geophys Res Lett* 33, L06405, doi:10.1029/2005GL025583.
33. da Rocha HR, et al. (2009) Patterns of water and heat flux across a biome gradient from tropical forest to savanna in Brazil. *J Geophys Res-Bioge* 114, G00B12, doi:10.1029/2007JG000640.

34. Humphreys ER, et al. (2006) Carbon dioxide fluxes in coastal Douglas-fir stands at different stages of development after clearcut harvesting. *Agr Forest Meteorol* 140(1-4):6-22.
35. McCaughey JH, Pejam MR, Arain MA, & Cameron DA (2006) Carbon dioxide and energy fluxes from a boreal mixedwood forest ecosystem in Ontario, Canada. *Agr Forest Meteorol* 140(1-4):79-96.
36. Flanagan LB & Adkinson AC (2011) Interacting controls on productivity in a northern Great Plains grassland and implications for response to ENSO events. *Global Change Biol* 17(11):3293-3311.
37. Dunn AL, Barford CC, Wofsy SC, Goulden ML, & Daube BC (2007) A long-term record of carbon exchange in a boreal black spruce forest: means, responses to interannual variability, and decadal trends. *Global Change Biol* 13(3):577-590.
38. Lafleur PM, Roulet NT, Bubier JL, Frolking S, & Moore TR (2003) Interannual variability in the peatland-atmosphere carbon dioxide exchange at an ombrotrophic bog. *Global Biogeochemical Cycles* 1036, doi:10.1029/2002GB001983, 2.
39. Goulden ML, et al. (2004) Diel and seasonal patterns of tropical forest CO₂ exchange. *Ecol Appl* 14(4):S42-S54.
40. Black TA, et al. (2000) Increased carbon sequestration by a boreal deciduous forest in years with a warm spring. *Geophys Res Lett* 27(9):1271-1274.
41. Howard EA, Gower ST, Foley JA, & Kucharik CJ (2004) Effects of logging on carbon dynamics of a jack pine forest in Saskatchewan, Canada. *Global Change Biol* 10(8):1267-1284.
42. Giasson MA, Coursolle C, & Margolis HA (2006) Ecosystem-level CO₂ fluxes from a boreal cutover in eastern Canada before and after scarification. *Agr Forest Meteorol* 140(1-4):23-40.
43. Bergeron O, et al. (2007) Comparison of carbon dioxide fluxes over three boreal black spruce forests in Canada. *Global Change Biol* 13(1):89-107.
44. Mkhabela MS, et al. (2009) Comparison of carbon dynamics and water use efficiency following fire and harvesting in Canadian boreal forests. *Agr Forest Meteorol* 149(5):783-794.
45. Zha T, et al. (2009) Carbon sequestration in boreal jack pine stands following harvesting. *Global Change Biol* 15(6):1475-1487.
46. Peichl M & Arain MA (2007) Allometry and partitioning of above- and belowground tree biomass in an age-sequence of white pine forests. *Forest Ecol Manag* 253(1-3):68-80.
47. Yuan FM, et al. (2008) Modeling analysis of primary controls on net ecosystem productivity of seven boreal and temperate coniferous forests across a continental transect. *Global Change Biol* 14(8):1765-1784.
48. Flanagan LB & Syed KH (2011) Stimulation of both photosynthesis and respiration in response to warmer and drier conditions in a boreal peatland ecosystem. *Global Change Biol* 17(7):2271-2287.
49. Adkinson AC, Syed KH, & Flanagan LB (2011) Contrasting responses of growing season ecosystem CO₂ exchange to variation in temperature and water table depth in two

- 703 peatlands in northern Alberta, Canada. *J Geophys Res-Biogeosci* 116, G01004,
704 doi:10.1029/2010JG001512.
- 705 50. Ammann C, Flechard CR, Leifeld J, Neftel A, & Fuhrer J (2007) The carbon budget of
706 newly established temperate grassland depends on management intensity. *Agr Ecosyst*
707 *Environ* 121(1-2):5-20.
- 708 51. Dietiker D, Buchmann N, & Eugster W (2010) Testing the ability of the DNDC model to
709 predict CO₂ and water vapour fluxes of a Swiss cropland site. *Agr Ecosyst Environ*
710 139(3):396-401.
- 711 52. Li X, et al. (2012) Estimation of evapotranspiration over the terrestrial ecosystems in
712 China. *Ecohydrology*. 7: 139–149.
- 713 53. Guan DX, et al. (2006) CO₂ fluxes over an old, temperate mixed forest in northeastern
714 China. *Agr Forest Meteorol* 137(3-4):138-149.
- 715 54. Yan Y, et al. (2008) Closing the carbon budget of estuarine wetlands with tower-based
716 measurements and MODIS time series (vol 14, pg 1690, 2008). *Global Change Biol*
717 14(10):2469-2471.
- 718 55. Chen SP, et al. (2009) Energy balance and partition in Inner Mongolia steppe ecosystems
719 with different land use types. *Agr Forest Meteorol* 149(11):1800-1809.
- 720 56. Kato T, et al. (2006) Temperature and biomass influences on interannual changes in CO₂
721 exchange in an alpine meadow on the Qinghai-Tibetan Plateau. *Global Change Biol*
722 12(7):1285-1298.
- 723 57. Sun G, et al. (2011) A general predictive model for estimating monthly ecosystem
724 evapotranspiration. *Ecohydrology* 4(2):245-255.
- 725 58. Sulkava M, Luyssaert S, Zaehle S, & Papale D (2011) Assessing and improving the
726 representativeness of monitoring networks: The European flux tower network example. *J*
727 *Geophys Res-Biogeosci* 116, G00J04, doi:10.1029/2010JG001562.
- 728 59. Staudt K & Foken T (2007) Documentation of reference data for the experimental areas
729 of the bayreuth centre for ecology and environmental research (bayceer) at the waldstein
730 site, Tech. Rep (University of Bayreuth).
- 731 60. Anthoni PM, et al. (2004) Forest and agricultural land-use-dependent CO₂ exchange in
732 Thuringia, Germany. *Global Change Biol* 10(12):2005-2019.
- 733 61. Knohl A, Schulze ED, Kolle O, & Buchmann N (2003) Large carbon uptake by an
734 unmanaged 250-year-old deciduous forest in Central Germany. *Agr Forest Meteorol*
735 118(3-4):151-167.
- 736 62. Schindler D, Turk M, & Mayer H (2006) CO₂ fluxes of a Scots pine forest growing in
737 the warm and dry southern upper Rhine plain, SW Germany. *Eur J Forest Res*
738 125(3):201-212.
- 739 63. Don A, Rebmann C, Kolle O, Scherer-Lorenzen M, & Schulze ED (2009) Impact of
740 afforestation-associated management changes on the carbon balance of grassland. *Global*
741 *Change Biol* 15(8):1990-2002.
- 742 64. Grunwald T & Bernhofer C (2007) A decade of carbon, water and energy flux
743 measurements of an old spruce forest at the Anchor Station Tharandt. *Tellus B*
744 59(3):387-396.

- 745 65. Rebmann C, et al. (2010) Treatment and assessment of the CO₂-exchange at a complex
746 forest site in Thuringia, Germany. *Agr Forest Meteorol* 150(5):684-691.
- 747 66. Pilegaard K, et al. (2003) Field measurements of atmosphere-biosphere interactions in a
748 Danish beech forest. *Boreal Environ Res* 8(4):315-333.
- 749 67. Gockede M, et al. (2008) Quality control of CarboEurope flux data - Part 1: Coupling
750 footprint analyses with flux data quality assessment to evaluate sites in forest
751 ecosystems. *Biogeosciences* 5(2):433-450.
- 752 68. Suni T, et al. (2003) Long-term measurements of surface fluxes above a Scots pine forest
753 in Hyytiälä, southern Finland, 1996-2001. *Boreal Environ Res* 8(4):287-301.
- 754 69. Laurila T, et al. (2001) Seasonal variations of net CO₂ exchange in European Arctic
755 ecosystems. *Theor Appl Climatol* 70(1-4):183-201.
- 756 70. Aurela M, et al. (2007) CO₂ exchange of a sedge fen in southern Finland - The impact of
757 a drought period. *Tellus B* 59(5):826-837.
- 758 71. Tanja S, et al. (2003) Air temperature triggers the recovery of evergreen boreal forest
759 photosynthesis in spring. *Global Change Biol* 9(10):1410-1426.
- 760 72. Hibbard KA, Law BE, Reichstein M, & Sulzman J (2005) An analysis of soil respiration
761 across northern hemisphere temperate ecosystems. *Biogeochemistry* 73(1):29-70.
- 762 73. Granier A, et al. (2000) The carbon balance of a young Beech forest. *Funct Ecol*
763 14(3):312-325.
- 764 74. Berbigier P, Bonnefond JM, & Mellmann P (2001) CO₂ and water vapour fluxes for 2
765 years above Euroflux forest site. *Agr Forest Meteorol* 108(3):183-197.
- 766 75. Rambal S, Joffre R, Ourcival JM, Cavender-Bares J, & Rocheteau A (2004) The growth
767 respiration component in eddy CO₂ flux from a *Quercus ilex* mediterranean forest.
768 *Global Change Biol* 10(9):1460-1469.
- 769 76. Bonal D, et al. (2008) Impact of severe dry season on net ecosystem exchange in the
770 Neotropical rainforest of French Guiana. *Global Change Biol* 14(8):1917-1933.
- 771 77. Nagy Z, et al. (2007) The carbon budget of semi-arid grassland in a wet and a dry year in
772 Hungary. *Agr Ecosyst Environ* 121(1-2):21-29.
- 773 78. Pinter K, et al. (2008) Interannual variability of grasslands' carbon balance depends on
774 soil type. *Community Ecol* 9:43-48.
- 775 79. Hirano T, et al. (2007) Carbon dioxide balance of a tropical peat swamp forest in
776 Kalimantan, Indonesia. *Global Change Biol* 13(2):412-425.
- 777 80. Peichl M, Leahy P, & Kiely G (2011) Six-year stable annual uptake of carbon dioxide in
778 intensively managed humid temperate grassland. *Ecosystems* 14(1):112-126.
- 779 81. Morales P, et al. (2005) Comparing and evaluating process-based ecosystem model
780 predictions of carbon and water fluxes in major European forest biomes. *Global Change*
781 *Biol* 11(12):2211-2233.
- 782 82. Kutsch WL, et al. (2010) The net biome production of full crop rotations in Europe. *Agr*
783 *Ecosyst Environ* 139(3):336-345.
- 784 83. Scartazza A, et al. (2004) Comparisons of $\delta^{13}\text{C}$ of photosynthetic products and
785 ecosystem respiratory CO₂ and their responses to seasonal climate variability. *Oecologia*
786 140(2):340-351.

- 787 84. Garbulsky MF, Penuelas J, Papale D, & Filella I (2008) Remote estimation of carbon
788 dioxide uptake by a Mediterranean forest. *Global Change Biol* 14(12):2860-2867.
- 789 85. Marcolla B, Pitacco A, & Cescatti A (2003) Canopy architecture and turbulence
790 structure in a coniferous forest. *Bound-Lay Meteorol* 108(1):39-59.
- 791 86. Marcolla B & Cescatti A (2005) Experimental analysis of flux footprint for varying
792 stability conditions in an alpine meadow. *Agr Forest Meteorol* 135(1-4):291-301.
- 793 87. Vaccari FP, et al. (2012) Land use change and soil organic carbon dynamics in
794 Mediterranean agro-ecosystems: The case study of Pianosa Island. *Geoderma* 175:29-36.
- 795 88. Migliavacca M, et al. (2009) Modeling gross primary production of agro-forestry
796 ecosystems by assimilation of satellite-derived information in a process-based model.
797 *Sensors-Basel* 9(2):922-942.
- 798 89. Montagnani L, et al. (2009) A new mass conservation approach to the study of CO₂
799 advection in an alpine forest. *J Geophys Res-Atmos* 114, D07306,
800 doi:10.1029/2008JD010650.
- 801 90. Rey A, et al. (2002) Annual variation in soil respiration and its components in a coppice
802 oak forest in Central Italy. *Global Change Biol* 8(9):851-866.
- 803 91. Tedeschi V, et al. (2006) Soil respiration in a Mediterranean oak forest at different
804 developmental stages after coppicing. *Global Change Biol* 12(1):110-121.
- 805 92. Chiesi M, et al. (2005) Modelling carbon budget of Mediterranean forests using ground
806 and remote sensing measurements. *Agr Forest Meteorol* 135(1-4):22-34.
- 807 93. Saito M, Miyata A, Nagai H, & Yamada T (2005) Seasonal variation of carbon dioxide
808 exchange in rice paddy field in Japan. *Agr Forest Meteorol* 135(1-4):93-109.
- 809 94. Ito A, et al. (2006) Seasonal variation in leaf properties and ecosystem carbon budget in
810 a cool-temperate deciduous broad-leaved forest: simulation analysis at Takayama site,
811 Japan. *Ecol Res* 21(1):137-149.
- 812 95. Takagi K, et al. (2009) Change in CO₂ balance under a series of forestry activities in a
813 cool-temperate mixed forest with dense undergrowth. *Global Change Biol* 15(5):1275-
814 1288.
- 815 96. Hirano T, et al. (2003) CO₂ and water vapor exchange of a larch forest in northern Japan.
816 *Tellus B* 55(2):244-257.
- 817 97. Choi M, Lee SO, & Kwon H (2010) Understanding of the Common Land Model
818 performance for water and energy fluxes in a farmland during the growing season in
819 Korea. *Hydrol Process* 24(8):1063-1071.
- 820 98. Kang M, Kwon H, Cheon JH, & Kim J (2012) On estimating wet canopy evaporation
821 from deciduous and coniferous forests in the Asian monsoon climate. *J Hydrometeorol*
822 13(3):950-965.
- 823 99. Jacobs CMJ, et al. (2007) Variability of annual CO₂ exchange from Dutch grasslands.
824 *Biogeosciences* 4(5):803-816.
- 825 100. Dolman AJ, Moors EJ, & Elbers JA (2002) The carbon uptake of a mid latitude pine
826 forest growing on sandy soil. *Agr Forest Meteorol* 111(3):157-170.
- 827 101. Moors EJ, et al. (2010) Variability in carbon exchange of European croplands. *Agr*
828 *Ecosyst Environ* 139(3):325-335.

102. Chojnicki B, Urbaniak M, Józefczyk D, Augustin J, & Olejnik J (2007) Measurements of gas and heat fluxes at Rzecin wetland. *Wetlands: Monitoring, Modeling and Management*, edited by Okruszko, T., Maltby, E., Szatylowicz, J., Mirosław-Swiątek, D., and Kotowski, W:125-131.
103. Pital G, Rodrigues A, Mateus J, & Pereira J (2011) Reversing of seasonal patterns of carbon uptake in an eucalyptus stand in Portugal after drought and felling. *Forest Syst* 20(3):475-484.
104. Pereira J, et al. (2007) Net ecosystem carbon exchange in three contrasting Mediterranean ecosystems—the effect of drought. *Biogeosciences* 4:791-802.
105. Merbold L, et al. (2009) Artificial drainage and associated carbon fluxes (CO₂/CH₄) in a tundra ecosystem. *Global Change Biol* 15(11):2599-2614.
106. van der Molen MK, et al. (2007) The growing season greenhouse gas balance of a continental tundra site in the Indigirka lowlands, NE Siberia. *Biogeosciences* 4(6):985-1003.
107. Kurbatova J, Li C, Varlagin A, Xiao X, & Vygodskaya N (2008) Modeling carbon dynamics in two adjacent spruce forests with different soil conditions in Russia. *Biogeosciences* 5(4):969-980.
108. Marchesini LB, et al. (2007) Carbon balance assessment of a natural steppe of southern Siberia by multiple constraint approach. *Biogeosciences* 4(4):581-595.
109. Sagerfors J, et al. (2008) Annual CO₂ exchange between a nutrient-poor, minerotrophic, boreal mire and the atmosphere. *J Geophys Res-Biogeosci* 113, G01001, doi:10.1029/2006JG000306.
110. Eklundh L, Jin HX, Schubert P, Guzinski R, & Heliasz M (2011) An optical sensor network for vegetation phenology monitoring and satellite data calibration. *Sensors-Basel* 11(8):7678-7709.
111. Lindroth A, Klemedtsson L, Grelle A, Weslien P, & Langvall O (2008) Measurement of net ecosystem exchange, productivity and respiration in three spruce forests in Sweden shows unexpectedly large soil carbon losses. *Biogeochemistry* 89(1):43-60.
112. Lagergren F, et al. (2008) Biophysical controls on CO₂ fluxes of three Northern forests based on long-term eddy covariance data. *Tellus B* 60(2):143-152.
113. Hargreaves K, Milne R, & Cannell M (2003) Carbon balance of afforested peatland in Scotland. *Forestry* 76(3):299-317.
114. Soussana JF, et al. (2007) Full accounting of the greenhouse gas (CO₂, N₂O, CH₄) budget of nine European grassland sites. *Agr Ecosyst Environ* 121(1-2):121-134.
115. Rebmann C, et al. (2005) Quality analysis applied on eddy covariance measurements at complex forest sites using footprint modelling. *Theor Appl Climatol* 80(2-4):121-141.
116. Wilkinson M, Eaton EL, Broadmeadow MSJ, & Morison JIL (2012) Inter-annual variation of carbon uptake by a plantation oak woodland in south-eastern England. *Biogeosciences* 9(12):5373-5389.
117. Acreman MC, Harding RJ, Lloyd CR, & McNeil DD (2003) Evaporation characteristics of wetlands: experience from a wet grassland and a reedbed using eddy correlation measurements. *Hydrol Earth Syst Sc* 7(1):11-21.

- 871 118.Kwon HJ, Oechel WC, Zulueta RC, & Hastings SJ (2006) Effects of climate variability
872 on carbon sequestration among adjacent wet sedge tundra and moist tussock tundra
873 ecosystems. *J Geophys Res-Bioge* 111, G03014, doi:10.1029/2005JG000036.
- 874 119.Jenkins JP, et al. (2007) Refining light-use efficiency calculations for a deciduous forest
875 canopy using simultaneous tower-based carbon flux and radiometric measurements. *Agr*
876 *Forest Meteorol* 143(1-2):64-79.
- 877 120.Gilmanov TG, et al. (2005) Integration of CO₂ flux and remotely-sensed data for primary
878 production and ecosystem respiration analyses in the Northern Great Plains: potential for
879 quantitative spatial extrapolation. *Global Ecol Biogeogr* 14(3):271-292.
- 880 121.Goldstein AH, et al. (2000) Effects of climate variability on the carbon dioxide, water,
881 and sensible heat fluxes above a ponderosa pine plantation in the Sierra Nevada (CA).
882 *Agr Forest Meteorol* 101(2-3):113-129.
- 883 122.Liu HP, Randerson JT, Lindfors J, & Chapin FS (2005) Changes in the surface energy
884 budget after fire in boreal ecosystems of interior Alaska: An annual perspective. *J*
885 *Geophys Res-Atmos* 110, D13101, doi:10.1029/2004JD005158.
- 886 123.Meyers TP & Hollinger SE (2004) An assessment of storage terms in the surface energy
887 balance of maize and soybean. *Agr Forest Meteorol* 125(1-2):105-115.
- 888 124.Oechel WC, et al. (2000) Acclimation of ecosystem CO₂ exchange in the Alaskan Arctic
889 in response to decadal climate warming. *Nature* 406(6799):978-981.
- 890 125.Pataki DE & Oren R (2003) Species differences in stomatal control of water loss at the
891 canopy scale in a mature bottomland deciduous forest. *Adv Water Resour* 26(12):1267-
892 1278.
- 893 126.Heinsch FA, et al. (2004) Carbon dioxide exchange in a high marsh on the Texas Gulf
894 Coast: effects of freshwater availability. *Agr Forest Meteorol* 125(1-2):159-172.
- 895 127.Urbanski S, et al. (2007) Factors controlling CO₂ exchange on timescales from hourly to
896 decadal at Harvard Forest. *J Geophys Res-Bioge* 112, G02020,
897 doi:10.1029/2006JG000293.
- 898 128.Hollinger DY, Aber J, & Dail B (2004) Spatial and temporal variability in forest-
899 atmosphere CO₂ exchange (vol 10, pg 1689, 2004). *Global Change Biol* 10(11):1961-
900 1961.
- 901 129.Allison VJ, Miller RM, Jastrow JD, Matamala R, & Zak DR (2005) Changes in soil
902 microbial community structure in a tallgrass prairie chronosequence. *Soil Sci Soc Am J*
903 69(5):1412-1421.
- 904 130.Powell TL, et al. (2006) Environmental controls over net ecosystem carbon exchange of
905 scrub oak in central Florida. *Agr Forest Meteorol* 141(1):19-34.
- 906 131.Borken W, Savage K, Davidson EA, & Trumbore SE (2006) Effects of experimental
907 drought on soil respiration and radiocarbon efflux from a temperate forest soil. *Global*
908 *Change Biol* 12(2):177-193.
- 909 132.Law BE, Thornton PE, Irvine J, Anthoni PM, & Van Tuyl S (2001) Carbon storage and
910 fluxes in ponderosa pine forests at different developmental stages. *Global Change Biol*
911 7(7):755-777.
- 912 133.Schmid HP, Grimmer CSB, Cropley F, Offerle B, & Su HB (2000) Measurements of
913 CO₂ and energy fluxes over a mixed hardwood forest in the mid-western United States.
914 *Agr Forest Meteorol* 103(4):357-374.

- 915 134.Sun G, et al. (2010) Energy and water balance of two contrasting loblolly pine
916 plantations on the lower coastal plain of North Carolina, USA. *Forest Ecol Manag*
917 259(7):1299-1310.
- 918 135.Noormets A, et al. (2010) Energy and water balance of two contrasting loblolly pine
919 plantations on the lower coastal plain of North Carolina, USA (vol 259, pg 1299, 2010).
920 *Forest Ecol Manag* 260(1):169-169.
- 921 136.Verma SB, et al. (2005) Annual carbon dioxide exchange in irrigated and rainfed maize-
922 based agroecosystems. *Agr Forest Meteorol* 131(1-2):77-96.
- 923 137.Monson RK, et al. (2002) Carbon sequestration in a high-elevation, subalpine forest.
924 *Global Change Biol* 8(5):459-478.
- 925 138.DeForest JL, et al. (2006) Phenophases alter the soil respiration-temperature relationship
926 in an oak-dominated forest. *Int J Biometeorol* 51(2):135-144.
- 927 139.Davis KJ, et al. (2003) The annual cycles of CO₂ and H₂O exchange over a northern
928 mixed forest as observed from a very tall tower. *Global Change Biol* 9(9):1278-1293.
- 929 140.Lipson DA, Wilson RF, & Oechel WC (2005) Effects of elevated atmospheric CO₂ on
930 soil microbial biomass, activity, and diversity in a chaparral ecosystem. *Appl Environ*
931 *Microb* 71(12):8573-8580.
- 932 141.Powell TL, et al. (2008) Carbon exchange of a mature, naturally regenerated pine forest
933 in north Florida. *Global Change Biol* 14(11):2523-2538.
- 934 142.Clark KL, Gholz HL, & Castro MS (2004) Carbon dynamics along a chronosequence of
935 slash pine plantations in north Florida. *Ecol Appl* 14(4):1154-1171.
- 936 143.Potts DL, Scott RL, Cable JM, Huxman TE, & Williams DG (2008) Sensitivity of
937 Mesquite Shrubland CO₂ Exchange to Precipitation in Contrasting Landscape Settings.
938 *Ecology* 89(10):2900-2910.
- 939 144.Desai AR, Bolstad PV, Cook BD, Davis KJ, & Carey EV (2005) Comparing net
940 ecosystem exchange of carbon dioxide between an old-growth and mature forest in the
941 upper Midwest, USA. *Agr Forest Meteorol* 128(1-2):33-55.
- 942 145.Ma SY, Baldocchi DD, Xu LK, & Hehn T (2007) Inter-annual variability in carbon
943 dioxide exchange of an oak/grass savanna and open grassland in California. *Agr Forest*
944 *Meteorol* 147(3-4):157-171.
- 945 146.Gough CM, Vogel CS, Schmid HP, Su HB, & Curtis PS (2008) Multi-year convergence
946 of biometric and meteorological estimates of forest carbon storage. *Agr Forest Meteorol*
947 148(2):158-170.
- 948 147.Wilson KB & Baldocchi DD (2001) Comparing independent estimates of carbon dioxide
949 exchange over 5 years at a deciduous forest in the southeastern United States. *J Geophys*
950 *Res-Atmos* 106(D24):34167-34178.
- 951 148.Cook BD, et al. (2004) Carbon exchange and venting anomalies in an upland deciduous
952 forest in northern Wisconsin, USA. *Agr Forest Meteorol* 126(3-4):271-295.
- 953 149.Noormets A, Chen J, & Crow TR (2007) Age-dependent changes in ecosystem carbon
954 fluxes in managed forests in northern wisconsin, USA. *Ecosystems* 10(2):187-203.
- 955 150.Sun G, Noormets A, Chen J, & McNulty SG (2008) Evapotranspiration estimates from
956 eddy covariance towers and hydrologic modeling in managed forests in Northern
957 Wisconsin, USA. *Agr Forest Meteorol* 148(2):257-267.

- 958 151.Scott RL, Hamerlynck EP, Jenerette GD, Moran MS, & Barron-Gafford GA (2010)
959 Carbon dioxide exchange in a semidesert grassland through drought-induced vegetation
960 change. *J Geophys Res-Bioge* 115, G03026, doi:10.1029/2010JG001348.
- 961 152.Falk M, Wharton S, Schroeder M, Ustin S, & U KTP (2008) Flux partitioning in an old-
962 growth forest: seasonal and interannual dynamics. *Tree Physiol* 28(4):509-520.
- 963 153.Navarro M, et al. (2008) Fruit development, not GPP, drives seasonal variation in NPP in
964 a tropical palm plantation. *Tree Physiol* 28(11):1661-1674.
- 965 154.Xiao X, Biradar C, Wang A, Sheldon S, & Chen Y (2011) Recovery of Vegetation
966 Canopy After Severe Fire in 2000 at the Black Hills National Forest, South Dakota,
967 USA. *Journal of Resources and Ecology* 2(2):106-116.
- 968 155.Ciais P, et al. (2005) Europe-wide reduction in primary productivity caused by the heat
969 and drought in 2003. *Nature* 437(7058):529-533.